

On the influence of collisional rate coefficients on the water vapour excitation

F. Daniel¹, J.R. Goicoechea¹, J. Cernicharo¹, M.-L. Dubernet^{2,3}, A. Faure⁴

¹ Departamento de Astrofísica, Centro de Astrobiología, CSIC-INTA, Ctra. de Torrejón a Ajalvir km 4, 28850 Madrid, Spain; e-mail: daniel@cab.inta-csic.es

² Observatoire de Paris, LUTH UMR CNRS 8102, 5 Place Janssen, 92195 Meudon, France

³ Université Pierre et Marie Curie, LPMAA UMR CNRS 7092, Case 76, 4 Place Jussieu, 75252 Paris Cedex 05, France

⁴ UJF-Grenoble 1/CNRS-INSU, Institut de Planétologie et d'Astrophysique de Grenoble (IPAG) UMR 5274, Grenoble F-38041, France

Received ...; accepted ...

ABSTRACT

Context. Water is a key molecule in many astrophysical studies that deal with star and planet forming regions, evolved stars and galaxies. Its high dipole moment makes this molecule to be subthermally populated under the typical conditions of most astrophysical objects. This motivated the calculation of various sets of collisional rate coefficients (CRC) for H₂O (with He or H₂) which are necessary to model its rotational excitation and line emission.

Aims. The most accurate set of CRC are the quantum rates that involve H₂. However, they were published only recently and less accurate CRC (quantum with He or quantum classical trajectory (QCT) with H₂) were used in many studies. This work aims to underline the impact that the new available set of CRC have on the interpretation of water vapour observations.

Methods. We performed accurate non-local non-LTE radiative transfer calculations using different sets of CRC in order to predict the line intensities from transitions that involve the lowest energy levels of H₂O (E < 900 K). The results obtained from the different CRC sets are then compared using line intensity ratio statistics.

Results. For the whole range of physical conditions considered in this work, we obtain that the intensities based on the quantum and QCT CRC are in good agreement. However, at relatively low H₂ volume density ($n(\text{H}_2) < 10^7 \text{ cm}^{-3}$) and low water abundance ($\chi(\text{H}_2\text{O}) < 10^{-6}$), these physical conditions being relevant to describe most molecular clouds, we find differences in the predicted line intensities of up to a factor of ~ 3 for the bulk of the lines. Most of the recent studies interpreting early Herschel Space Observatory spectra used the QCT CRC. Our results show that although the global conclusions from those studies will not be drastically changed, each case has to be considered individually, since depending on the physical conditions, the use of the QCT CRC may lead to a mis-estimate of the water vapour abundance of up to a factor of ~ 3 . Additionally, the comparison of the quantum state-to-state and thermalized CRC that include the description of the population of the H₂ rotational levels show that above $T_K \sim 100 \text{ K}$, large differences are expected from those two sets for the p-H₂ symmetry. Finally, we have found that at low temperature (i.e. $T_K < 100 \text{ K}$) modelled line intensities will be differentially affected by the symmetry of the H₂ molecule. If a significant number of H₂O lines is observed, it is therefore possible to obtain an estimate of the H₂ ortho-to-para ratio from the analysis of the line intensities.

Key words. Line: formation ; Molecular data ; Radiative transfer ; Radiation mechanisms: thermal ; ISM: abundances ; ISM: molecules

1. Introduction

Water is a key molecule for both the chemistry and the cooling budget along the star formation trail. The determination of the water vapour abundance is a long standing problem in astrophysics. Because water vapour is predicted to be an abundant molecule in the gas phase, the determination of its spatial extent, its distribution, and its abundance is crucial in modelling the chemistry and the physics of molecular clouds, comets, evolved stars and galaxies (Neufeld & Kaufman, 1993; Neufeld et al., 1995; Cernicharo & Crovisier, 2005; van Dishoeck et al., 2011). In warm molecular clouds, water vapour can play a critical role in the gas cooling (Neufeld & Kaufman, 1993; Neufeld et al., 1995) and, hence, in the evolution of these objects.

Unfortunately, water is an abundant molecule in our atmosphere making particularly difficult the observation of its rotational lines and vibrational bands from Earth. Even so, some observations of H₂O maser lines have been performed from ground-based and airborne telescopes: the $6_{16} - 5_{23}$ at 22 GHz

(Cheung et al., 1969), the $5_{15} - 4_{22}$ at 325 GHz (Menten et al., 1990a), the $10_{29} - 9_{36}$ at 321 GHz (Menten et al., 1990b) and the $3_{13} - 2_{20}$ at 183.31 GHz (Waters et al., 1980; Cernicharo et al., 1990, 1994). The spectrometers on board the *Infrared Space Observatory* (Kessler et al., 1996) provided a unique opportunity to observe infrared (IR¹) H₂O thermal lines in a great variety of astronomical environments. Several studies demonstrated that water emission is a unique tracer of the warm gas and energetic processes taking place during star formation (see reviews

¹ Throughout this article, many acronyms are used. While defined in the article when first introduced, they are compiled here for clarity :

- IR: infrared
- CRC: collisional rate coefficients
- STS : state-to-state
- RT: radiative transfer
- QCT: quantum classical trajectory
- OTPR : ortho-to-para ratio

by van Dishoeck (2004) and Cernicharo & Crovisier (2005)). In particular, ISO observations showed that far-IR H₂O emission lines are important coolants of the warm gas affected by shocks (e.g., more than 70 pure rotational lines were detected towards Orion KL outflows; Cernicharo et al. 2006a) confirming earlier theoretical predictions of its importance in the shocked gas cooling (e.g., Neufeld & Kaufman, 1993). ISO also detected widespread H₂O absorption towards the Galactic Center (e.g., Goicoechea et al., 2004) and towards the nucleus of more distant galaxies (e.g., Gonzalez-Alfonso et al., 2004). After ISO, the launch of both the *Submillimeter Wave Astronomy Satellite*, SWAS (Melnick et al., 2000), and *ODIN* (Nordh et al., 2003) allowed the observation of the $1_{10} - 1_{01}$ fundamental transition of both H₂¹⁶O (at 557 GHz) and H₂¹⁸O (at 548 GHz, first detected by the *Kuiper Airborne Observatory*; Zmuidzinas et al. 1995) at high heterodyne spectral resolution but poor angular resolution. Their resolved line-profiles (line-wing emission, widths, self-absorption dips, etc.) were studied in detail. Finally, the *Spitzer Space Telescope* has detected even higher excitation H₂O pure rotational lines (up to $E_u \approx 3000$ K) in the shocked gas around protostars (albeit at low spectral resolution; e.g., Watson et al. 2007).

The HIFI and PACS spectrometers on board *Herschel Space Observatory* (Pilbratt et al., 2010) provide much higher sensitivity and angular/resolution than previous far-IR observations, allowing us to detect a larger number of excited H₂O lines in many more sources, and to better constrain the spatial origin of the water vapour emission. The *HIFISTARS*² key project has addressed the problem of the water abundance in evolved stars and complement with high spectral resolution the results obtained previously by the Infrared Space Observatory (ISO). Similar goals, but covering a much larger spectral domain with lower spectral resolution, have been addressed by the *MESS* (Mass-loss of Evolved StarS³) key project. The *WISH* (Water In Star forming regions with Herschel⁴) key project focussed on the study of young stellar objects in different evolutionary stages. Early Herschel results include the detection of strong H₂O emission in protostellar environments (e.g., van Dishoeck et al., 2011); the presence of water vapour in diffuse interstellar clouds with an *ortho-to-para* ratio (OTPR) consistent with the high temperature ratio of 3 (Lis et al., 2010), the detection of cold water vapour in TW Hydrae protoplanetary disk with a low OTPR of ≈ 0.8 (Hogerheijde et al., 2011) and the widespread occurrence of H₂O in circumstellar envelopes around O-rich and C-rich evolved stars (Royer et al., 2010; Neufeld et al., 2011). In the outflows of Class 0 protostars, for example, tens of pure rotational lines of water vapour (up to $9_{18} - 9_{09}$ or $E_u \approx 1500$ K) are readily detected in the far-IR domain (Herczeg et al., 2012; Goicoechea et al., 2012).

In order to derive the water vapour abundance and to estimate the prevailing physical conditions in the above environments, the energy level excitation and the radiative transfer (RT) of H₂O lines has to be understood. H₂O is an asymmetric molecule with a irregular set of energy levels characterised by quantum numbers $J_{K_A K_C}$. Because of the large rotation constants of H₂O, its pure rotational transitions lie in the submm and far-IR domain. Their high critical densities (much higher than CO lines) and large optical-depths often results in a complex non-local and non-LTE excitation and RT problem. In addition, in sources with strong far-IR continuum emission, radiative pumping by warm

dust photons can play an important role in determining the rotational levels population (e.g., Cernicharo et al., 2006b).

Most of the information which is made available through water lines observations rely on modelling its excitation. From this point of view, water is difficult molecule to treat since its high dipole moment makes most of its transitions to be subthermally excited (see, e.g., Cernicharo et al. (2006b)), harbouring very large opacities (see, e.g., González-Alfonso et al. (1998)), many of them being maser in nature (Cheung et al., 1969; Waters et al., 1980; Phillips et al., 1980; Menten et al., 1990a,b; Menten & Melnick, 1991; Cernicharo et al., 1990, 1994; Cernicharo et al., 1996, 1999; Cernicharo et al., 2006b; González-Alfonso et al., 1995, 1998). An accurate modelling thus require, in addition to a good description of the source structure, the availability of accurate collisional rate coefficients. In the case of saturated masers a special formalism has to be developed in order to take into account saturation effects and to solve the RT problem (Daniel & Cernicharo, 2012). To summarise, the water vapour abundance in different environments can change by orders of magnitude (e.g., van Dishoeck et al., 2011) and H₂O rotational line profiles are sensitive probes of the gas kinematics and physical conditions (e.g., Kristensen et al., 2012). These facts make water vapour lines a powerful diagnostic tool in astrophysics.

The methodology used to compare two collisional rate coefficients sets is presented in Sect. 2 and a comparison between the various sets available for H₂O is given in Sect. 3. A discussion on the effect introduced by the H₂ ortho-to-para ratio is presented in Sect. 4. Finally, we discuss the current results in Sect. 5 and the conclusions are drawn in Sect. 6.

2. Comparison between collisional rate coefficients sets: methodology

Water is a key molecule for both the chemistry and cooling budget of the warm molecular gas. The need to understand the excitation mechanisms leading to line formation motivated the determination of various collisional rate coefficients sets (hereafter referred as CRC) for this molecule.

The first water vapour CRC were calculated using He as a collisional partner, considered the first 45th rotational energy levels for both ortho- and para-H₂O and were calculated for temperatures in the range 20–2000 K (Green et al., 1993). Collisions with H₂ were subsequently determined (Phillips et al., 1996) making use of the 5D potential energy surface (PES) described in Phillips et al. (1994). This study showed that considering either ortho- or para-H₂ as a collisional partner could lead to substantial differences in the magnitude of the CRC. However, this study dealt with a limited number of H₂O energy levels (5 levels) and results were only made available for a reduced range of temperatures (20–140K). The latter calculations were extended to lower temperatures (to cover the range 5–20K) by Dubernet & Grosjean (2002) and Grosjean et al. (2003) making use of the same PES. The importance of water subsequently led to the calculation of a high precision 9D PES for the H₂O – H₂ system (Faure et al., 2005; Valiron et al., 2008). The influence of the results based on the latter PES (averaged over the vibration of H₂O and H₂ thus reducing the dimension to 5) with the previous PES (Phillips et al., 1994) are discussed in Dubernet et al. (2006). Using the latter PES, quantum classical trajectory (QCT) calculations were performed to determine CRC for the 45th first energy levels of H₂O for both ortho- and para-H₂ (Faure et al., 2007). The range of temperature covered by these calculations is 100–2000 K (note that CRC are provided below 100 K, making

² <http://hifistars.oan.es/>

³ <http://www.univie.ac.at/space/MESS/>

⁴ <http://www.strw.leidenuniv.nl/WISH/>

use of the quantum CRC of Dubernet et al. (2006) for the transitions that involve the lowest five energy levels of either o-H₂O or p-H₂O and assuming a constant temperature dependence for the other transitions.) Making use of laboratory measurements for the vibrational relaxation of water and QCT calculations (Faure et al., 2005), the QCT CRC of Faure et al. (2007), obtained for the vibrational ground state, have subsequently been scaled to provide ro-vibrational CRC for the 5th first vibrational states (Faure & Josselin, 2008). Finally, quantum calculations were performed for the H₂O – H₂ system making use of the same 5D PES than the one used in the QCT calculations. These quantum calculations provide CRC for the first 45th energy levels of both ortho and para H₂O and for temperatures covering the 5–1500K range (Dubernet et al., 2009; Daniel et al., 2010, 2011). In these latter studies, an emphasis is made on the inclusion of the excited energy levels of H₂. Therefore, apart from the usual state-to-state CRC commonly calculated in quantum studies (i.e. with H₂ remaining in its fundamental rotational level during the collision), the availability of the information relative to the H₂ excitation is used to determine thermalized CRC.

Owing to the time at which the different CRC sets were made available and owing to the number of energy levels considered and to the temperature coverage, the analysis of water excitation has mainly been based on three sets: the quantum H₂O – He CRC of Green et al. (1993), the QCT CRC of Faure et al. (2007) and the quantum CRC of Dubernet et al. (2006, 2009); Daniel et al. (2010, 2011). In what follows, we discuss the H₂O line intensity predictions based on these three CRC sets and calculated with a precise non-LTE non-local radiative transfer code. Additionally, we choose to focus the discussion only on the o-H₂O symmetry since the results are similar for the p-H₂O symmetry.

2.1. Radiative transfer modelling

We performed RT calculations using the various sets of CRC available for o-H₂O and p-H₂O. The numerical code used to solve the molecular excitation and the RT problem is described in Daniel & Cernicharo (2008). The water vapor spectroscopic parameters, i.e. line frequencies and Einstein coefficients, are taken from the HITRAN database (Rothman et al., 2009). The model consists of a static spherical homogeneous cloud with turbulence velocity dispersion fixed at 1 km s⁻¹ and with a radius of $\sim 4.5 \cdot 10^{16}$ cm (i.e. 6'' at 500 pc). Since we focus on collisional effects, pumping by the dust infrared radiation is not included in a first stage, so that the population of the water energy levels is only due to the collisions with the H₂ molecules and to radiative trapping due to line opacity effects. The inclusion of dust emission is however briefly discussed in Sect. 5. A grid of models has been run leaving the gas temperature, the H₂ volume density and the water abundance relative to H₂ as free parameters. Those quantities vary in the ranges : $T \in [200\text{K}; 1000\text{K}]$, $n(\text{H}_2) \in [10^6 ; 2 \cdot 10^9] \text{ cm}^{-3}$ and $\chi(\text{H}_2\text{O}) \in \{10^{-8}; 10^{-6}; 10^{-4}\}$, for both o-H₂O and p-H₂O. All the RT models are performed considering the first 45th energy levels of p-H₂O or o-H₂O, irrespective of the CRC set used.

Since we solve the non-local excitation problem, we consider an average of the parameters that describe the radiative transitions in order to compare the results based on the different CRC sets. Therefore, the influence of the CRC on the line emission is estimated from the quantity :

$$\bar{I}_j = B(T_{bg}) e^{-\tau_j} + B(\bar{T}_{ex}) \times (1 - e^{-\tau_j}) \quad (1)$$

where $B(T)$ stands for the Planck function, τ_j for the opacity at the j line center and T_{bg} is the temperature of the background radiation (set to the CMB temperature in what follows, except if specified). \bar{I}_j corresponds to the specific intensity of the transition j , along a ray with constant excitation conditions (i.e. constant \bar{T}_{ex}). The excitation temperature \bar{T}_{ex} is defined as an average over the N radial grid points of the models, and is calculated according to :

$$\bar{T}_{ex} = \frac{\mathcal{A}}{2} \sum_{i=1}^{N-1} [\kappa(r_i) T_{ex}(r_{i+1}) + \kappa(r_{i+1}) T_{ex}(r_i)] \times \frac{r_{i+1} - r_i}{r_N - r_1} \quad (2)$$

where r_i stands for the distance of the i^{th} grid point to the centre of the sphere, \mathcal{A} is a normalisation coefficient and $\kappa(r)$ is the j line absorption coefficient at radius r . Calculating \bar{T}_{ex} this way, we prevent that lines with suprathermal excitation (i.e. $T_{ex} > T_K$), but with nearly equal populations for the upper and lower levels, have their averaged \bar{T}_{ex} overestimated. Indeed, even under homogeneous conditions, most of the lines show large variations of $T_{ex}(r)$ at the edge of the sphere, which are in general associated with low values of the absorption coefficients. Weighting $T_{ex}(r)$ by the associated $\kappa(r)$ enables to reduce the influence of such variations and insure that its mean value is representative of the volume of the cloud which emits photons. The line opacity τ_j is given by :

$$\tau_j = \frac{1}{2} \sum_{i=1}^{N-1} [\kappa(r_i) + \kappa(r_{i+1})] \times (r_{i+1} - r_i) \quad (3)$$

The comparison of the various models is done using \bar{I}_j rather than using the line intensity peaks (noted $\max(I_j)$ in what follows) or the integrated area of the lines (noted W_j), for various reasons. At a first glance, the two latter estimators would result more natural, since such quantities would be the one used to compare observations and models. However, a difficulty arise from the fact that for a given line, the line profiles may differ from one model to the other. In such a case, the ratio obtained considering either $\max(I_j)$ or W_j can differ by a few 10%.

This is illustrated in Fig. 1. In this figure, the models considered correspond to the physical parameters : $T_K = 800$ K, $n(\text{H}_2) = 2 \cdot 10^7 \text{ cm}^{-3}$ and $\chi(\text{o-H}_2\text{O}) = 10^{-6}$. The collisional partner is p-H₂ and the results compared are obtained using the QCT CRC of Faure et al. (2007) and STS quantum CRC of Dubernet et al. (2009) (respectively labelled *QCT* and *quant.* in the following). These CRC sets are more extensively discussed in Sect. 3. The two bottom panels show the variation of $W_j^{\text{quant.}} / W_j^{\text{QCT}}$ (left panel) and $\max(I_j)^{\text{quant.}} / \max(I_j)^{\text{QCT}}$ (right panel) as a function of $\bar{I}_j^{\text{quant.}} / \bar{I}_j^{\text{QCT}}$. Considering the integrated intensity, it can be seen that most of the W_j and \bar{I}_j ratios show maximum differences of the order of 25 % (the two dashed lines on the left panel correspond to straight lines of slopes 0.75 and 1.25 and thus delimit a maximum deviation of 25 %.) Considering the peak intensity (right panel), it can be seen that the correlation between the $\max(I_j)$ and \bar{I}_j ratios is better than for the case of the integrated intensity. In that case, the maximum differences are lower than 10 % (the dashed lines correspond to straight lines of slopes 0.9 and 1.1). The four upper panels illustrate the fact that the three estimators start to lead to different ratios when the line profiles of the two models differ. In this figure, we report the brightness temperature for the impact parameter that crosses the center of the sphere. The profile obtained with the p-H₂ QCT CRC correspond to the black curves. The red curves correspond to the profiles obtained with the p-H₂ quantum CRC, and scaled by

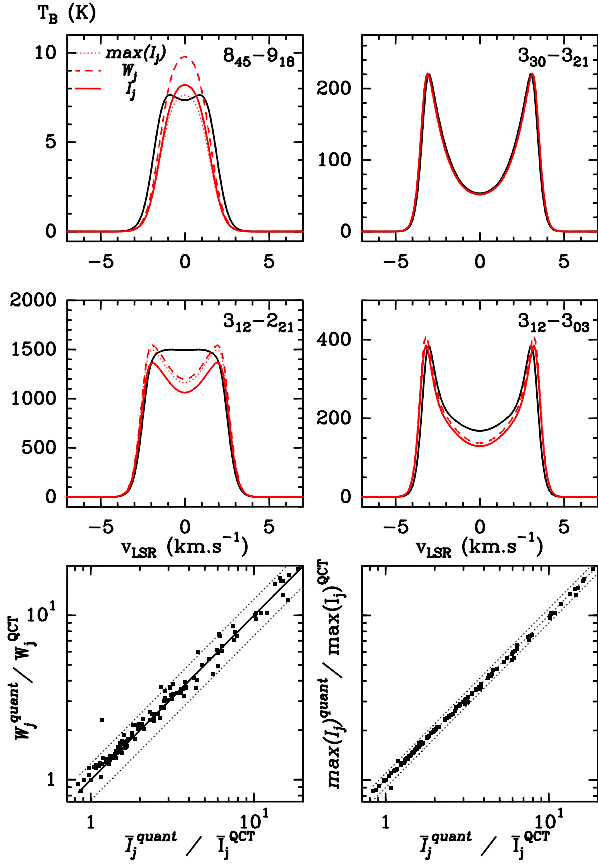


Fig. 1. Comparison of the line intensity ratios based on three estimators: \bar{I}_j , the integrated area W_j , or the peak intensity $\max(I_j)$ (see text for details). The four upper panels give the brightness temperature of a few o-H₂O lines. The black curve corresponds to the profile obtained with the quantum CRC set and the red curves to the QCT CRC set (see text for details). In the latter case, the profile is scaled according to the ratios of \bar{I}_j (plain curve), W_j (dashed curve) or $\max(I_j)$ (dotted curve) so that the profiles which are plotted would correspond to a ratio of unity according to the three estimators. The two bottom panels represent the variations of the ratios obtained between the various indicators and for all the lines of the model.

the ratio $\bar{I}_j^{\text{QCT}}/\bar{I}_j^{\text{quant}}$ (plain curve), $W_j^{\text{QCT}}/W_j^{\text{quant}}$ (dashed curve) and $\max(I_j)^{\text{QCT}}/\max(I_j)^{\text{quant}}$ (dotted curve). In other words, the red curves would correspond to line profiles that would lead to a ratio of unity, when compared to the black curve and depending on the estimator used. It can be seen that for the 3₃₀-3₂₁ line, since the line profiles derived from the two CRC sets are identical, the ratio obtained from the three estimators are identical too. On the other hand, for example for the 3₁₂-2₂₁ line, the three estimators lead to different ratios since the line profiles obtained using the two CRC sets differ.

Finally, we emphasize on the fact that in principle, whatever of the three estimators could be used in order to perform the comparisons which are presented in the next sections. The conclusions would not be affected by this choice due to the good correlation between the ratios obtained with those three estimators. We prefer to use \bar{I}_j because of its simplicity and because it reduces the line intensity simply to two parameters, the averaged excitation temperature and the line opacity, the first quantity being a useful indicator on how far the line is from thermalization.

2.2. Comparison of rate coefficient sets

In order to compare two CRC sets, noted SET1 and SET2, we consider the values taken by the ratios $x_j = \bar{I}_j^{\text{SET1}}/\bar{I}_j^{\text{SET2}}$, where \bar{I} is defined by eq. 1 and where the index j stands for the j^{th} radiative transition. The comparisons are made considering the statistics on the M radiative lines that respect the criteria:

- the line does not show substantial population inversion (i.e. we adopt as a selection criterium that the opacity of a line in the inverted region can not be greater than 0.5% of the opacity of the line in the thermal region.)
- the upper level of the line has an energy below the N^{th} level (labelled as N_{max} in what follows)
- the intensity of the line as given by eq. 1 is above 10 mK

The first criterium means that the masers are discarded from the statistical analysis. Hence, the following conclusions do not concern the lines observable with the ALMA interferometer. We refer to Daniel & Cernicharo (2012) for a discussion concerning the impact of the CRC on these masing lines. From these M lines, we define the mean (noted m) and standard deviation (noted σ) associated of the x_j ratios given by:

$$\sigma = \sqrt{\frac{1}{M} \sum_{j=1}^M (x_j - m)^2} \quad (4)$$

Additionally, we discuss the results using the normalised standard deviation defined as σ/m rather than σ .

3. Comparison between various H₂O CRC

In what follows, we discuss the H₂O line intensity predictions based on the three CRC sets which have been widely used, i.e. the quantum H₂O – He CRC of Green et al. (1993), the QCT CRC of Faure et al. (2007) and the quantum CRC of Dubernet et al. (2006, 2009); Daniel et al. (2010, 2011).

3.1. o-H₂O QCT and quantum STS CRC with H₂ compared to quantum He CRC

In this section, various comparisons are made between the quantum state-to-state (STS) CRC calculated with either p-H₂ (Dubernet et al., 2009; Daniel et al., 2011) or o-H₂ (Daniel et al., 2011), the quantum STS CRC calculated with He (Green et al., 1993) and the QCT calculations (Faure et al., 2007). When referring to the quantum H₂ STS CRC, it is assumed that the CRC stands for the CRC where H₂ remains in its fundamental rotational energy level (i.e. either $j_2 = 0$ for p-H₂ or $j_2 = 1$ for o-H₂ with j_2 being the H₂ rotational quantum number). Note that QCT rate coefficients are not STS but obtained for thermal populations of p-H₂ and o-H₂, i.e. they are thermalized CRC (see below). In the RT calculations, the CRC calculated with He are scaled according to the differing reduced masses of the H₂O–He and H₂O–H₂ systems, in order to emulate collisions with H₂.

3.1.1. p-H₂ rate coefficients

A first comparison is made between the o-H₂O/p-H₂ CRC sets obtained with the quantum calculations and the QCT calculations, both with respect to the quantum calculations performed with He. The mean and normalised standard deviations of the ratios $\bar{I}^{\text{H}_2}/\bar{I}^{\text{He}}$ are represented on Fig. 2 for various water abundances and considering the o-H₂O lines with upper energy levels

below the 20th level ($E_u < 900$ K). It appears that the behaviour of the x_j ratios can be distinguished between two regimes, which are separated by a threshold (noted n in what follows) in the water volume density $n(\text{H}_2\text{O}) = n(\text{H}_2) \times \chi(\text{H}_2\text{O})$. For water volume densities $n(\text{H}_2) \times \chi(\text{H}_2\text{O}) > n$, the mean value is around 1 and the normalised standard deviation takes low values (typically below 0.1). This corresponds to the *thermalized regime* where the line intensity ratios are basically independent of the adopted CRC set. In this regime, most of the lines show large optical depths. These large optical depths imply that the critical densities of the lines become lower than in the optically thin limit⁵, hence producing the thermalization of the level populations. For $n(\text{H}_2) \times \chi(\text{H}_2\text{O}) < n$, the level populations are determined by both collisional and radiative processes, making the mean value differing from 1 and leading to an increase of the normalised standard deviation (in what follows, this regime is referred as *subthermal regime*).

In Fig. 2 we show a comparison of the line intensity ratios obtained with the quantum p-H₂ CRC (left column) and QCT p-H₂ CRC (right column), both compared to the quantum He CRC. Examining the p-H₂ CRC, we see that independently of the abundance considered, the mean value is in the range $0.45 < m < 1.35$. The normalised standard deviation is below 0.5 for all the free parameter space, which means that most of the lines (roughly 70% of the lines considered) show deviations of less than 50% around the mean value. In other words, the main effect introduced by considering the H₂ CRC will be to scale the line intensities with respect to the intensities derived from the He CRC. The maximum difference in the scaling factor is encountered at high temperature and low H₂ volume densities, where the line intensities based on the H₂ CRC are found to be lower by a factor around ~ 2 , for $\chi(\text{H}_2\text{O}) = 10^{-8}$. Additionally, the relative line intensities are expected to vary from one set to the other, with maximum variations of the order of 50% for the bulk of the lines.

The QCT calculations show slightly larger differences, as expected since they correspond to thermalized CRC. Indeed, we obtain that irrespective of the water vapour abundance, the mean value of the ratios is in the range $1 < m < 2.9$, for the whole parameter space considered here. The normalised standard deviation can take values of up to ~ 0.7 . The spread of the ratio around the mean value is of the same order than the one found for the quantum p-H₂ CRC.

In Fig. 4 (right column), we show a direct comparison of the results predicted by the STS and QCT CRC. Independently of the water abundance, the QCT CRC predict larger intensities (a factor 2 higher) than the STS CRC. This is due to the fact that the QCT calculations correspond to a thermal average over the H₂ energy levels and because of the large differences of the CRC for H₂ in its fundamental state $j_2 = 0$ and in the $j_2 = 2$ state. This is further discussed when considering the thermalized CRC (see Sect. 3.2).

3.1.2. o-H₂ rate coefficients

A second comparison concerns the results obtained with o-H₂ as a collisional partner. The results obtained with the quantum and QCT CRC are compared to the results obtained with He in Fig. 3. Qualitatively, the H₂ quantum and QCT calculations compares similarly to the results obtained with He. The main ef-

fect concerns the overall scaling of the ratios. In the subthermal regime, the intensity ratios obtained using o-H₂ are higher than the one obtained using He, irrespective of the water abundance. A typical increase of 50% is found for the intensity of the lines, with mean values that can be higher than 3 in the regime of low temperatures and low densities. This result is expected from a direct consideration of CRC obtained with o-H₂. Indeed, these rates are typically higher than the rates with He, by factors of up to a factor 10. So, the water energy levels are more easily populated when considering o-H₂ as a collisional partner. This results in brighter lines. Additionally, we note that the normalised standard deviation is high and its variations are correlated with the variations of the mean value, i.e. the higher the mean value is, the higher the normalised standard deviation is.

A direct comparison of the results obtained with the quantum and QCT calculations is shown in Fig. 4 for o-H₂ (left column). The differences found for the intensities are modest as long as the water abundance is such that $\chi(\text{H}_2\text{O}) \geq 10^{-6}$. In that case, the mean value is found to be around 1 and the normalised standard deviation is below 0.3 for all the parameter space. The main differences are found for $n(\text{H}_2) < 10^7 \text{ cm}^{-3}$ and $\chi(\text{H}_2\text{O}) \sim 10^{-8} \text{ cm}^{-3}$ where mean values in the range $1.5 < m < 2$ are obtained.

3.2. Quantum thermalized CRC with QCT or STS CRC

In this section, we compare the intensities predicted using the quantum state-to-state CRC with the one derived using the thermalized CRC (both defined in Dubernet et al., 2009; Daniel et al., 2011), defined as :

$$R_{ij} = \sum_{j_2} n(j_2) \sum_{j'_2} C_{ij}(j_2 \rightarrow j'_2) \quad (5)$$

In this expression, $C_{ij}(j_2 \rightarrow j'_2)$ stands for the state-to-state CRC from state i to state j for the H₂O molecule and that corresponds to the transition $j_2 \rightarrow j'_2$ for the H₂ molecule. These thermalized CRC thus consider the possibility of energy transfer for both the target molecule (H₂O in the present case) and the collider. The populations of the H₂ energy levels [noted $n(j_2)$ in the above expression] are assumed to be in thermal equilibrium, so that the populations are given by the Boltzmann distribution. In principle, any astrophysical study should consider thermalized rather than STS CRC when dealing with line excitation. In practice, the H₂O molecule (and its isotopomers in Faure et al., 2012) is the only molecule for which thermalized CRC have been calculated with a quantum approach. In what follows, we will emphasise on the effects introduced by considering thermalized rather than STS CRC, keeping in mind that the current findings obtained for the case of water vapour can be extrapolated to other molecules.

The thermalized CRC differ from the quantum STS CRC in two ways. In the following discussion, we consider the case of the collisions with p-H₂. At low temperature (i.e. $T \leq 50$ K), only the fundamental level of the p-H₂ molecule is substantially populated. The thermalized CRC thus reduce to $R_{ij} \sim C_{ij}(0 \rightarrow 0) + C_{ij}(0 \rightarrow 2)$. At low temperature, the second term of this expression is often negligible compared to the first term, except for the H₂O transitions for which the variation of the energy induced by the collision is higher than the energy necessary to excite the p-H₂ molecule to its first excited state. In the case of p-H₂, this corresponds to transitions that satisfy $\Delta E_{ij} > 500$ K. For these transitions, the term $C_{ij}(0 \rightarrow 2)$ starts to be dominant in the evaluation of the thermalized CRC since such a rate can be higher by

⁵ i.e. $n_c = A_{ul} \langle \beta \rangle / C_{ul}$ where β is the probability that a photon escapes the medium ; with $\beta = 1$ in the optically thin case and $\beta \sim 1/\tau$ when the line becomes optically thick

up to a factor 10 in comparison to the STS CRC where H₂ remains in its fundamental level. The main effect induced by this process is to efficiently populate the H₂O energy levels for the levels with energies higher than 500 K. This is illustrated in Fig. 5, for a model with parameters $n(\text{H}_2) = 10^6 \text{ cm}^{-3}$, $T_K = 50 \text{ K}$ and $\chi(\text{H}_2\text{O}) = 10^{-4}$. In this figure, we report the water vapour level populations averaged over radius. It can be seen that for the levels with energies below 500 K, the STS and thermalized CRC give similar results for the level populations. On the other hand, for the levels with energies higher than 500 K, the populations obtained using the thermalized CRC are globally 10 times higher than the one obtained from the STS CRC. Note that in

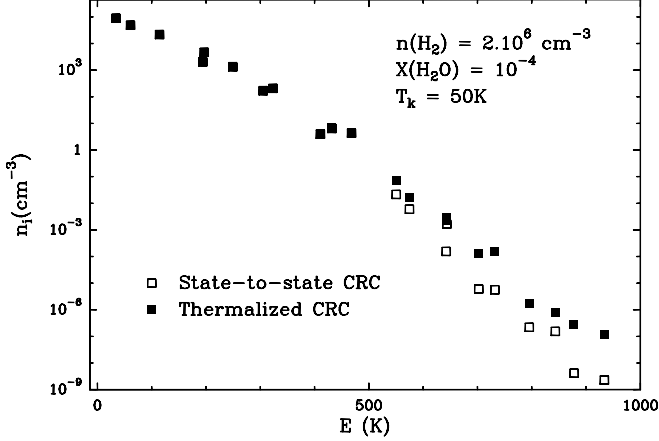


Fig. 5. Populations of the o-H₂O energy levels as a function of the level energy, for a model with parameters : $n(\text{H}_2) = 10^6 \text{ cm}^{-3}$, $T_K = 50 \text{ K}$ and $\chi(\text{H}_2\text{O}) = 10^{-4}$. The populations obtained with the state-to-state CRC correspond to the open boxes whereas the one obtained with the thermalized CRC correspond to the filled boxes.

the case of low temperatures, these differences are irrelevant for any astrophysical study since the levels higher than 500 K correspond to transitions which are far below the detection limit of the current telescopes. This example is however given to emphasize the effect introduced by the terms $C_{ij}(0 \rightarrow 2)$, the same effect being found at higher temperatures. However, at higher temperatures, the transitions from the $j_2 = 2$ state make the influence of those terms less evident when considering the level populations, as discussed below.

At higher temperature, the first p-H₂ excited state starts to be substantially populated. Collisions from the state $j_2 = 2$ thus influence the evaluation of the thermalized CRC. In this case, all the H₂O transitions are affected by the scaling of the CRC due to the term $n(j_2 = 2) \times C_{ij}(2 \rightarrow 2)$. In the case of the H₂O molecule, the term $C_{ij}(2 \rightarrow 2)$ is globally larger than $C_{ij}(0 \rightarrow 0)$ by a factor that ranges from 2 to 10 depending on the transition. Consequently, the thermalized CRC for all the transitions are globally increased since at the temperatures of 100, 200, 500 K, the population of the $j_2 = 2$ state account for 3, 28 and 58% of the total p-H₂ molecules respectively. As an example, at 200 K, all the thermalized CRC are increased by factors in the range 1.5–3.5 depending on the transition. Additionally, as discussed in the case of the low temperatures, the CRC for the transitions with $\Delta_{ij} > 500 \text{ K}$ will be increased due to the term $C_{ij}(0 \rightarrow 2)$.

Finally, Fig. 6 shows a comparison of the results based on thermalized and STS CRC, for temperatures in the range 20–100

K and for the 10th first o-H₂O rotational energy levels. From this figure, it appears that the temperature at which the thermalized CRC start to influence the line intensities is around $T_K \sim 60 \text{ K}$.

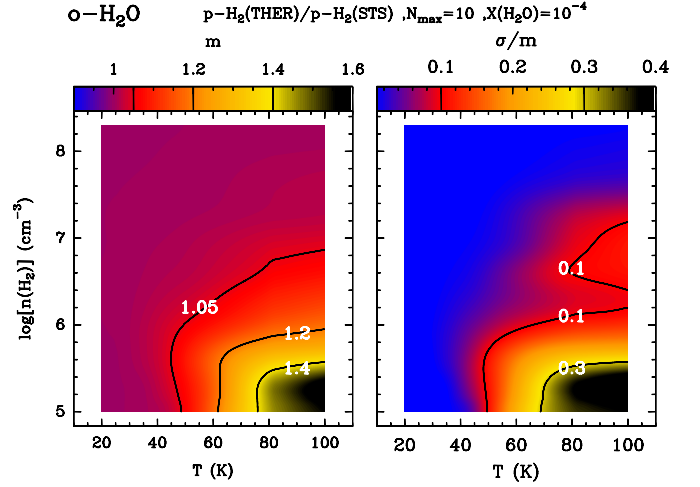


Fig. 6. Comparison of the results based on the thermalized and STS CRC from Dubernet et al. (2009); Daniel et al. (2011) for gas temperatures in the range 20–100 K and for a water abundance $\chi(\text{H}_2\text{O}) = 10^{-4}$.

3.2.1. Comparison of the thermalized, STS and QCT CRC

In Fig. 7, we compare the quantum STS (Dubernet et al., 2009; Daniel et al., 2011) and QCT (Faure et al., 2007) CRC with the results obtained with the thermalized CRC for p-H₂ (Dubernet et al., 2009; Daniel et al., 2011). It can be seen that adopting the thermalized CRC strongly influences the results. Indeed, in the limit of low density (i.e. $n(\text{H}_2) < 10^7 \text{ cm}^{-3}$), both STS and QCT CRC give results that can differ by more than a factor 3, if we consider the mean value. Such high differences are found over all the temperatures considered here for what concerns the STS CRC. On the other hand, the differences between the QCT and thermalized CRC decrease with temperature. Above 400 K, the mean value obtained from the comparison of the QCT and thermalized CRC is below 2.

In Fig. 8, we compare the results based on thermalized and STS (Daniel et al., 2011) CRC for the o-H₂ symmetry. In this figure, we see that the thermalized CRC give similar results than the STS CRC, with a mean value in the range $1 < m < 1.2$ and normalized standard deviation below 0.15 for all the parameter space. The results are shown for a water abundance $\chi(\text{H}_2\text{O}) = 10^{-8}$ but the results are similar for other abundances. The similarity of the derived line intensities is due to the fact that the terms $C_{ij}(j_2 \rightarrow j'_2)$ that involve the $j_2 = 1$ state or $j_2 = 3$ state are similar in magnitude.

Fig. 9 show the $\bar{I}^{THER}/\bar{I}^{QCT}$ ratios for both o-H₂ and p-H₂, for eight H₂O transitions commonly observed with the HIFI and PACS spectrometers on-board Herschel. For each line, the ratios for the prediction based on the o-H₂ set are given in the left panel, while the ratios obtained from the CRC that involve p-H₂ are given in the right one. Note the similarity of the intensity ratio obtained for both the o-H₂ and p-H₂ symmetries. This behaviour will be further discussed in the Sect. 4. The figure corresponds to a water abundance $\chi(\text{H}_2\text{O}) = 10^{-8}$. From this figure, it appears that the two CRC sets will lead to qualitatively

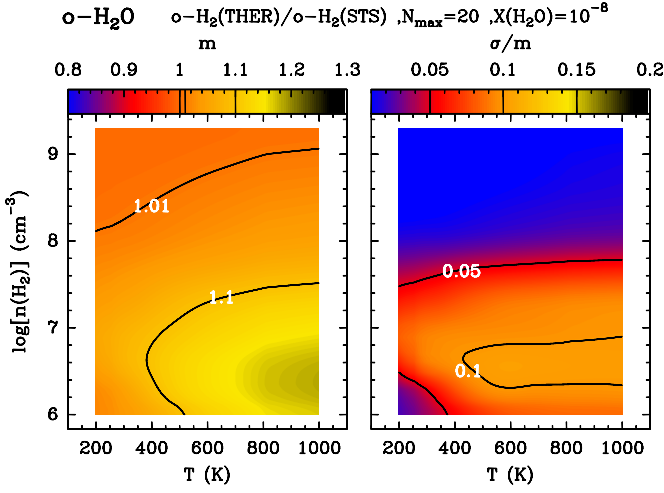


Fig. 8. Comparison of the results based on the thermalized and STS CRC from Daniel et al. (2011), for o-H₂ and for gas temperatures in the range 200–1000 K and for a water abundance $\chi(\text{H}_2\text{O}) = 10^{-8}$.

similar predictions for the line intensities. Indeed, the maximum variations which are found are of the order of a factor of 3, in the worst case. For the lines considered here, and considering collisions with o-H₂ (the most abundant symmetry for H₂ in hot media), the o-H₂O lines that show the largest differences (i.e. greater than a factor of ~ 2) are the $1_{10} - 1_{01}$, $2_{21} - 2_{12}$, $3_{30} - 2_{21}$ lines. These differences are found at $n(\text{H}_2) < 10^7 \text{ cm}^{-3}$ and for all the temperatures considered here. On the other hand, some lines show only small variations from one set to the other, with intensities that agree within 20% (e.g. $2_{12} - 1_{01}$; $3_{03} - 2_{12}$; $3_{12} - 3_{03}$; $4_{14} - 3_{03}$). Moreover, we find that for the majority of the lines, the predictions based on the QCT CRC give lower intensities for the o-H₂ symmetry (for all the lines except the $3_{12} - 3_{03}$ for which a ratio between 0.6 and 0.8 are found at high temperatures). This implies that an analysis based on the QCT CRC will tend to underestimate the water abundance.

3.2.2. Behaviour of the thermalized CRC

A striking feature, when considering the comparison of the STS and thermalized CRC arises from the behaviour at low temperature. Indeed, the highest differences are found in the range 200–400 K between those sets. Simply considering the fact that the population of the p-H₂ $j_2 = 2$ level increases with temperature, one would expect the differences between those two sets to behave similarly, to reach a maximum when the fundamental level is depopulated. On the contrary, the highest differences are found around 200 K and tend to diminish while the temperature increases. This effect is due to the terms $C_{ij}(j_2 \rightarrow j'_2)$ with $\Delta j_2 \geq 2$. In order to quantify the influence of those terms, we used an ad-hoc set of CRC. In this set, the thermalized CRC are calculated setting to 0 all the CRC with $\Delta j_2 \neq 0$. The comparison between the results based on the STS, QCT and thermalized CRC with this ad-hoc set is shown in Fig. 10. The comparison is made at a density $n(\text{H}_2) = 2.10^7 \text{ cm}^{-3}$ and for a water abundance $X(\text{H}_2\text{O}) = 10^{-8}$. The choice of these parameters is based on the results shown in Fig. 7 where it can be seen that for both the QCT and STS CRC, these parameters correspond to the maximum differences encountered. Considering the mean value obtained for the ratio

$\bar{I}^{\text{ther}} / \bar{I}^{\text{approx}}$, we see that the mean value has its maximum at 200 K and then decreases with temperature. This proves that the terms $C_{ij}(j_2 \rightarrow j'_2)$ with $\Delta j_2 \geq 2$ are responsible of the high differences encountered at low temperatures. Considering the mean value for the ratios $\bar{I}^{\text{QCT}} / \bar{I}^{\text{approx}}$, we find that it has a constant value ~ 1.0 over the whole temperature range. The normalized standard deviation decreases from 0.4 to 0.3 as the temperature increases. In other words, the ad-hoc set of CRC and the QCT CRC give the same results within $\sim 30\%$. This shows that the main drawback of the QCT approximation is that it does not correctly reproduce the terms $C_{ij}(0 \rightarrow 2)$. This result is not surprising since these transitions have large rate coefficients when there is a quasi-resonance between the H₂O and H₂ rotational levels, i.e. transitions with $\Delta_{ij} > 500 \text{ K}$. At the QCT level, quasi-resonant effects are not included properly owing to the approximate quantization procedure.

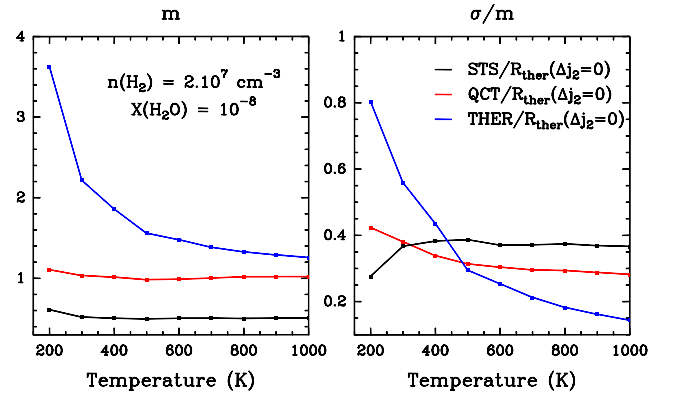


Fig. 10. Comparison of the mean (left column) and normalized standard deviation (right column) obtained for the ratios $\bar{I} / \bar{I}^{\text{approx}}$ and dealing with p-H₂. The approximation consists in neglecting the terms $C_{ij}(j_2 \rightarrow j'_2)$ with $\Delta j_2 \geq 2$ in the calculation of the thermalized CRC. The results obtained with this approximation are compared to the quantum state-to-state CRC (black lines) from Dubernet et al. (2009); Daniel et al. (2011), the QCT CRC (red lines) from Faure et al. (2007) and thermalized CRC (blue lines) from Dubernet et al. (2009); Daniel et al. (2011).

3.3. Discussion

In the previous sections, we compared the results of various CRC sets for o-H₂O. The comparisons were made by considering the lines that involve energy levels below the 20th one (i.e. $E_u < 900 \text{ K}$). With respect to the water symmetry, calculations were also performed for the p-H₂O molecule and the conclusions were found to be similar, i.e. the quantum thermalized and QCT CRC give qualitatively similar results for the line intensities, when considering both o-H₂ and p-H₂ as collisional partners, with maximum differences for the bulk of the lines of the order of a factor 3.

With respect to the number of H₂O levels considered, a similar statistical analysis has been performed considering the lines that involve the first 35th energy levels. The differences for the ratios were found to be larger for the lines with $E_u > 900 \text{ K}$. This qualitatively results in larger variations of the normalised standard deviations (i.e. would magnify the scale of σ on Fig.

2, 3 and 4). This is illustrated on Fig. 11 where the mean value and standard deviations are given, for the ratio between the o-H₂ STS and QCT CRC. In this figure, we consider all the lines with energy level below the 35th level and for the case of a water abundance of $\chi(\text{H}_2\text{O}) = 10^{-6}$. The results are to be compared to the results shown on Fig. 4 where only the first 20th levels were considered.

Finally, to a first order, it can be seen that the variations of intensities from one set to the other are linearly correlated to the CRC variations. This is illustrated by considering the critical densities related to the various sets of CRC discussed in the previous sections which are reported in Table 1. Comparing, as an example, the critical densities related to the p-H₂ QCT and thermalized CRC, we can see that the maximum differences is of a factor 3, which is similar to the maximum difference found for the intensity ratio (see Sect. 3.2).

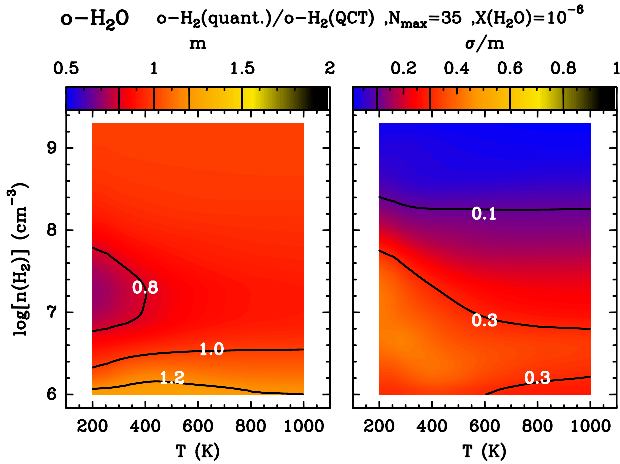


Fig. 11. Mean value and normalised standard deviation obtained comparing the quantum CRC from Dubernet et al. (2009); Daniel et al. (2011) and QCT CRC from Faure et al. (2007), for a water abundance of $\chi(\text{H}_2\text{O}) = 10^{-6}$ cm⁻³. The lines retained in the comparison have an energy below the one of the 35th level of o-H₂O.

4. The o-H₂ / p-H₂ dichotomy

To date, apart from H₂O, only a few collisional systems have been treated considering both o-H₂ and p-H₂ as collisional partners (i.e. CO by Wernli et al. (2006), HC₃N by Wernli et al. (2007), SiS by Lique & Klos (2008); Klos & Lique (2008), H₂CO by Troscompt et al. (2009), HNC by Dumouchel et al. (2011), CN⁻ by Klos & Lique (2011), SO₂ by Cernicharo et al. (2011), HF by Guillon & Stoecklin (2012), HDO by Faure et al. (2012)). Except in the CN⁻ case, a common conclusion is that the o-H₂ CRC are larger than for p-H₂. In the particular case of water, the differences are rather large, with CRC for o-H₂ that can be larger by up to a factor 10 compared to p-H₂. This implies that the population of the high energy levels through collisions with o-H₂ will be favoured. To date, only few detailed discussions concerning the differences in the excitation of a given molecule and considering the effects introduced by the differing collisional partners exist. A short discussion of the influence of the H₂ OTPR ratio was made by Cernicharo et al. (2009), where a few water vapour lines were considered for the

case of a model describing a protoplanetary disk. Such a discussion has also been done for the H₂CO molecule. Troscompt et al. (2009) found that the H₂ OTPR was crucial in explaining the excitation of the 1₁₀ – 1₁₁ line, and that it is possible to accurately constrain the H₂ OTPR ratio from its observation. On the other hand, Guzmán et al. (2011) found that for the physical conditions which are typical of the Horsehead nebula, the H₂CO lines observed in their study are insensitive to the H₂ OTPR. A similar conclusion was obtained by Parise et al. (2011) for the deuterated isotopomers of H₃⁺ which were found to be marginally affected by the H₂ OTPR for the conditions typical of prestellar cores (see also Pagani et al. (2009)). In what follows, we discuss some characteristics of the water vapour excitation with respect to collisions with o-H₂ or p-H₂.

In order to study the influence of the H₂ symmetry, we compare the ratio of the values taken by \bar{I} for the quantum CRC (i.e. $\bar{I}_{ortho}/\bar{I}_{para}$). In the comparison, we consider both the STS and thermalized CRC. For a given line, we compute the mean value and the normalised standard deviation by summing over all the the models that correspond to the parameter space defined in Sec. 2. We use the same selection for the lines as previously done and which are given by the criteria indicated in Sec. 2.

4.1. State-to-State rate coefficients

The mean value and normalised standard deviation are plotted in Fig. 12, for the three value of the water abundance considered in this work. In this figure, we see that the mean value and normalised standard deviation will depend differently on the collisions with o-H₂ or p-H₂ according to the energy of the upper level involved in the transition. Additionally, there is a correlation between the sensitivity of the transition to the o-H₂ / p-H₂ symmetry with the position of the upper energy level on the J-ladder⁶. Qualitatively, an increase of the energy of the upper level will be accompanied by an increase of both the mean value and normalised standard deviation. For the transitions that involve an upper energy level below 500 K, we find that independently of the water abundance, the mean value is around 1 and the normalised standard deviation takes low values (below 1). Those lines are thus marginally affected by the collisional partner. For the lines with an upper energy level above 500 K, the transitions which are the less affected by the nature of the collisional partner are the transitions where the upper energy level is a backbone level (blue points in Fig. 12). For these transitions, the mean value remains relatively low (typically below 2.5) for all the values of the water abundance. The normalised standard deviation is minimal for those transitions, especially when the water abundance is low. This implies that the intensity of these transitions will be only marginally affected by the symmetry of the collisional partner. The transitions which are the most affected are the one for which the upper level is not a backbone level while the lower level is backbone level (red points in Fig. 12). These transitions should be good indicators of the H₂ OTPR of the gas.

⁶ As a reminder, H₂O is an asymmetric top with quantum numbers noted either J, K_a, K_c or J, K_+, K_- . A backbone level corresponds to the lower level in energy for a given value of the principal quantum number J . This level corresponds to the lowest possible value for the difference $K_a - K_c$.

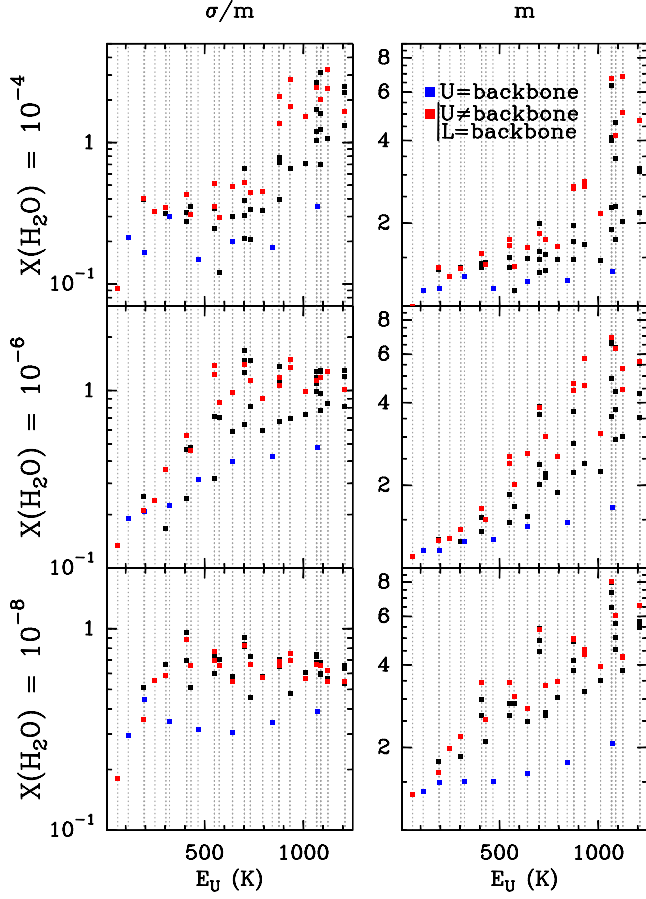


Fig. 12. Mean value (left column) and normalised standard deviation (right column) for the $\bar{I}_{ortho}/\bar{I}_{para}$ ratios as a function of the energy of the upper level of the radiative transitions. The intensities are obtained with the STS CRC Dubernet et al. (2009); Daniel et al. (2011). The transitions that involve an upper energy level which is backbone are indicated by blue points. The transitions where the upper level is not a backbone level while the lower level is backbone are indicated by red points.

4.2. Thermalized rate coefficients

In the previous section, on the base of the quantum state-to-state CRC, it was shown that the H₂ OTPR would influence differentially the intensities of the water transitions. In this section, the same analysis is performed using the thermalized quantum CRC, for high gas temperatures ($T_k > 200$ K) and low gas temperatures ($T_k < 100$ K).

4.2.1. High temperature

Figure 13 shows the means and normalised standard deviations for the ratios $\bar{I}_{ortho}/\bar{I}_{para}$ obtained using the thermalized quantum CRC. From this figure, it appears that the bulk of the lines are mainly insensitive to the H₂ OTPR, contrary to what was obtained using the STS CRC. For the transitions that involve an upper energy level with energy below 500 K, the mean value is found to be close to 1, independently of the water abundance considered. For the transitions that involve higher levels, we find that there is a departure from the mean value of 1 but the departure is modest, since most of the intensity ratios are in the range $0.7 < m < 1.1$. Additionally, the normalised standard de-

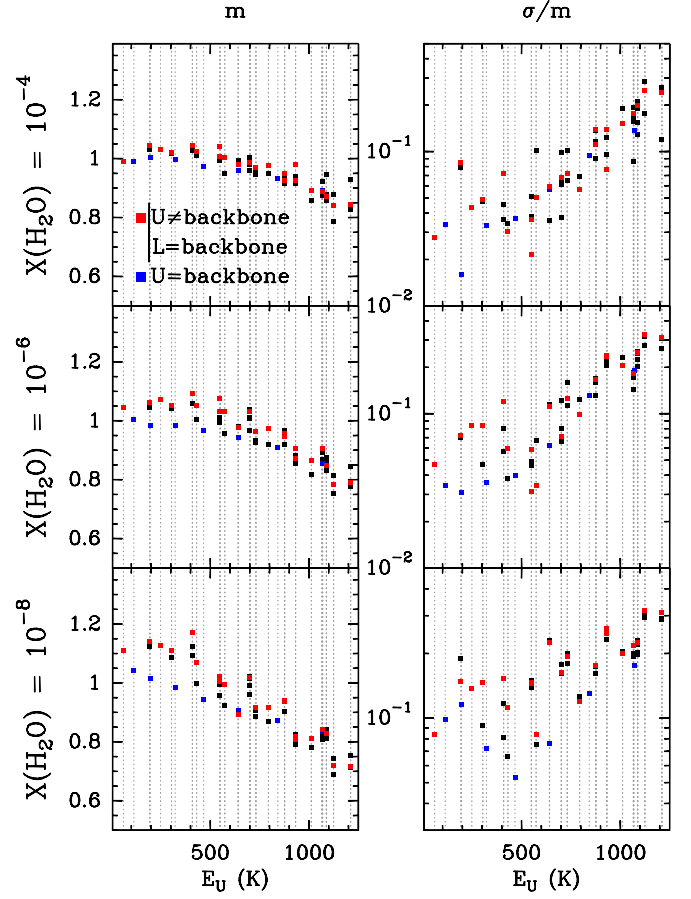


Fig. 13. Same as Fig. 12 but considering the quantum thermalized CRC from Dubernet et al. (2009); Daniel et al. (2011).

viations are low, i.e. $\sigma/m < 0.3$, which means that $\sim 70\%$ of the lines considered in the analysis show variations of less than 30% around the mean value. Interestingly, the transitions that involve energy levels higher than 500 K are found to be globally brighter when considering the collisions with p-H₂ than when considering the collisions with o-H₂. This effect is induced by the increase of magnitude of the CRC with $\Delta E_{ij} > 500$ K which has been discussed in Sec. 2.

4.2.2. Low temperatures

To discuss the low temperature regime, we carried out models with free parameters in the range : $T \in [20\text{K}; 100\text{K}]$, $n(\text{H}_2) \in [10^5; 2 \cdot 10^8] \text{ cm}^{-3}$ and $\chi(\text{H}_2\text{O}) \in \{10^{-8}; 10^{-6}; 10^{-4}\}$. The mean values and normalised standard deviations are calculated for each line by considering all the models of the grid. In Table 2, we give the mean values and standard deviations for all the lines. From this table, it appears that all the lines which are considered are affected by the H₂ OTPR. The main effect, as discussed earlier, is to obtain an increase of intensity when considering o-H₂ as a collisional partner, for the transitions with upper energy level below 500 K. On the other hand, for the levels with an upper energy level above 500 K, considering p-H₂ as a collisional partner results in higher intensities. Additionally, the line intensities are affected differentially by the symmetry of the collisional partner. This differential effect is presented in Fig. 14 where the intensity ratios are shown for some of the lines that involve the lowest energy levels of o-H₂O. From this figure it can be seen that

under specific physical conditions, the intensity ratio can take high values for certain lines (i.e. larger than 15, like for example for the $2_{21} - 2_{12}$) while it remains low for other lines (i.e. below 2, like for example for the $4_{14} - 3_{03}$). Since, the lines depend differentially on the H₂ OTPR, it is in principle possible to determine the H₂ OTPR for the molecules of the gas from an accurate modelling of the water line intensities observations. In practice, however, this can be a difficult task due to the dependence of the line intensities on other parameters of the model, like the gas temperature, H₂ volume density and geometry of the source. Moreover, this is only feasible if it relies on a large set of observations. This puts strong limits on the usefulness of water to derive the H₂ OTPR at low temperature ($T < 50$ K) since only a few transitions will be observable with a reasonable sensitivity (i.e. with RMS < 10 mK).

5. Dust radiative pumping

All the comparisons performed in Sec. 2 and 3 were done ignoring the possibility of pumping by infrared and sub-millimetre dust radiation. This would correspond to an extreme case, not physically relevant to all astrophysical objects. Indeed, as an example, radiative pumping by continuum photons plays an important role in the H₂O excitation in AGB circumstellar envelopes. In short, considering this additional mechanism in the population of the water energy levels would reduce the differences between line intensities obtained from differing CRC. This is illustrated in Fig 15, where we consider the $\bar{I}^{ortho} / \bar{I}^{para}$ ratios obtained from the STS CRC. In this example, we choose to compare the results based on these CRC since it has been found in Sec. 4 that the respective intensities show large differences and thus enable to emphasize the role played by dust radiation. The model parameters are: $n(\text{H}_2) = 10^6 \text{ cm}^{-3}$, $T_K = 200 \text{ K}$ and $\chi(\text{H}_2\text{O}) = 10^{-8}$. In the model, we assume a gas-to-dust mass ratio of 100 and the dust composition corresponds to a mixture of astrophysical silicates and amorphous carbon grains, with opacities taken from Draine & Lee (1984). In the modelling, we varied the dust temperature (T_d) from 5 K to 200 K. Moreover, to compute \bar{I} , we assume for the background temperature: $T_{bg} = T_d$. From this figure, we see that while the mean values and standard deviations are high at low dust temperatures ($m \sim 7$ and $\sigma \sim 5$), they are considerably reduced when T_d increases. For dust temperatures above 50 K, we obtain $m \sim 1$ and $\sigma < 0.2$, which implies that the influence of differing CRC starts to be minimal since the population of the H₂O energy levels is dominated by radiative pumping and not by the collisions anymore.

6. Conclusions

We performed non-local non-LTE excitation and radiative transfer calculations aiming at comparing the line intensities predicted for water vapour when making use of differing collisional rate coefficients sets. The collisional rate coefficients sets compared are the He quantum rate coefficients (Green et al., 1993), H₂ quantum rate coefficients of (Dubernet et al., 2006, 2009; Daniel et al., 2010, 2011) and H₂ quasi-classical rate coefficients (Faure et al., 2007). The comparison was performed at relatively high temperature ($200 \text{ K} < T_K < 1000 \text{ K}$) and an emphasis was made on the comparison of the H₂ collisional rate coefficient sets, since the quantum rate coefficients were only made lately available and many recent astrophysical studies made use of the QCT calculations. In the absence of radiative pumping by dust photons, it was found that the results based on the quantum and

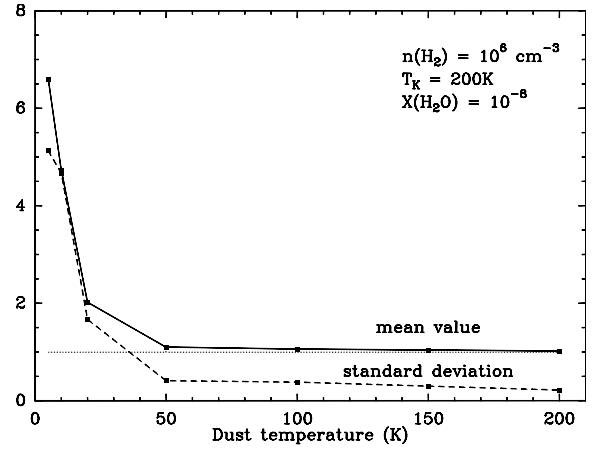


Fig. 15. Mean value and standard deviation as a function of the dust temperature. The ratio considered are obtained considering the quantum ortho- and para- STS CRC from Dubernet et al. (2009); Daniel et al. (2011).

QCT rate coefficients sets will lead to line intensities that qualitatively agree, i.e. which are of the same order of magnitude, for the parameter space considered in this work. However, the H₂O line emission can differ by a factor of the order of ~ 3 , in the regime of low water abundance ($\chi(\text{H}_2\text{O}) \sim 10^{-8}$) and moderate H₂ volume densities ($n(\text{H}_2) < 10^7 \text{ cm}^{-3}$).

These differences should not drastically affect the conclusions obtained from the modelling of the water excitation in astrophysical objects but the water vapour abundance derived on the base of the QCT rate coefficients will differ with the one derived from the quantum rate coefficients, with differences still up to a factor of ~ 3 . We note, however, that such differences will be attenuated by the presence of a dust continuum source of radiation. Additionally, masing lines are not considered in the present analysis. A similar comparison for the case of masing lines is presented in Daniel & Cernicharo (2012) where the impact induced by the CRC on the lines that will be observable with ALMA is discussed. Finally, we emphasize on the fact that the impact of the various CRC sets is discussed on the base of a statistics over the most intense lines. The current results can thus be affected to some extent by the choice of the subset of lines used in the analysis.

The differences found between the QCT and quantum CRC can give clues on the uncertainty which is introduced in the modeling due to the uncertainties on the rate coefficients. Indeed, as it was discussed in Dubernet et al. (2009) and Daniel et al. (2010), the QCT and quantum CRC typically agree within a factor of 3 for what concerns the highest rate coefficients. In the current study, we obtain the same factor between the line intensities obtained with two sets. Therefore, in a first approximation, the error made on the rate coefficients will translate similarly on line intensities. Recently, Yang et al. (2011) found a good agreement between experimental integral cross sections and quantum calculations, showing the good accuracy of the PES on which are based the quantum calculations. Depending on the energy of the level considered and the gas temperature, it was said in Dubernet et al. (2009) and Daniel et al. (2010) that the accuracy of the quantum CRC will range from a few % to a few ten % and such errors should scale linearly on line intensities.

We performed additional test calculations with an ad-hoc set of thermalised collisional rate coefficients in which the state-

to–state rate coefficients associated to the H₂ transitions with $\Delta j_2 \neq 0$ were removed. The comparison of the results obtained with this ad–hoc set and the QCT rate coefficients showed a particularly good agreement. Over the temperature range $T = 200\text{--}1000$ K, the intensities predicted with those two sets agree within 30%. It is concluded that the main drawback of the QCT approximation is that it does not correctly reproduce the terms $C_{ij}(0 \rightarrow 2)$.

By considering the quantum state–to–state and quantum thermalized collisional rate coefficients, it was found that line intensities will be largely affected by the consideration of the first excited state, in the case of p–H₂. The differences start to be non–negligible (i.e. greater than 20%) for temperatures higher than $T_K \sim 60$ K, reaching a maximum of a factor ~ 3 around 200 K. On the other hand, the intensities predicted with the state–to–state and thermalized collisional rate coefficients are similar for the collisions that involve o–H₂. Such a behaviour can be extrapolated to other molecules that show strong differences for the collisions between o–H₂ and p–H₂. Indeed, such differences arise because of the interaction with the quadrupole of H₂ and significant differences for the collisional rate coefficients with p–H₂ or o–H₂ imply that the state–to–state rate coefficients for p–H₂ in $j_2 = 0$ or $j_2 = 2$ will show large differences too. Therefore, the use of state–to–state rather than thermalized collisional rate coefficients for such molecules will lead to an overestimate of the molecular abundances for temperatures higher than $T_K \sim 60$ K.

By comparing the line intensities obtained using as a collisional partner either o–H₂ or p–H₂, we found that under particular physical conditions ($n(\text{H}_2)$ and T_K), the water lines will be differentially affected by the symmetry of the H₂ molecule. This effect is obtained when the gas temperature is low, i.e. $T_K < 100$ K. On the contrary, at high temperature, the lines become insensitive to the H₂ symmetry. Since some transitions will show large intensity variations with respect to the H₂ symmetry, the modelling of the water excitation may provide a mean to derive the H₂ ortho–to–para ratio. The lines to be considered in such an estimate will however depend on the physical conditions prevailing in the object under study and it is necessary to perform a case–by–case modelling.

Acknowledgements. The authors want to thank the anonymous referee whose detailed comments enabled to improve the content of the current article. This paper was partially supported within the programme CONSOLIDER INGENIO 2010, under grant "Molecular Astrophysics: The Herschel and ALMA Era-ASTROMOL" (Ref.: CSD2009- 00038). We also thank the Spanish MICINN for funding support through grants AYA2006-14876 and AYA2009-07304. JRG is supported by a Ramón y Cajal research contract from the Spanish MICINN and co-financed by the European Social Fund.

References

Cernicharo, J., Thum, C., Hein, H., John, D., Garcia, P., & Mattiocco, F. 1990, *A&A*, 231, L15
 Cernicharo, J., Gonzalez-Alfonso, E., Alcolea, J., Bachiller, R., & John, D. 1994, *ApJ*, 432, L59
 Cernicharo, J., González-Alfonso, E., Bachiller, R. 1996, *A&A*, 305
 Cernicharo, J., Pardo, E., Serabyn et al., 1999, *ApJ*, 520, L131
 Cernicharo, J., & Crovisier, J. 2005, *Space Sci. Rev.*, 119, 29
 Cernicharo, J., Goicoechea, J.R., Daniel, F. et al. 2006a, *ApJ*, 649L, 33
 Cernicharo, J., Goicoechea, J.R., Pardo, J.R., Asensio-Ramos, A. 2006b, *ApJ*, 642, 940
 Cernicharo, J., Ceccarelli, C., Ménard, F., Pinte, C., & Fuente, A. 2009, *ApJ*, 703, L123
 Cernicharo, J., Spielfiedel, A., Balança, C., et al. 2011, *A&A*, 531, A103
 Cheung, A. C., Rank, D. M., Townes, C. H., Thornton, D. D., & Welch, W. J. 1969, *Nature*, 221, 626
 Daniel, F., & Cernicharo, J. 2008, *A&A*, 488, 1237

Daniel, F., Dubernet, M.-L., Pacaud, F., & Grosjean, A. 2010, *A&A*, 517, A13
 Daniel, F., Dubernet, M.-L., & Grosjean, A. 2011, *A&A*, 536, A76
 Daniel, F., & Cernicharo, J. 2012, *A&A*, submitted
 Draine, B. T., & Lee, H. M. 1984, *ApJ*, 285, 89
 Dubernet, M.-L., & Grosjean, A. 2002, *A&A*, 390, 793
 Dubernet, M.-L., Daniel, F., Grosjean, A., et al. 2006, *A&A*, 460, 323
 Dubernet, M.-L., Daniel, F., Grosjean, A., & Lin, C. Y. 2009, *A&A*, 497, 911
 Dumouchel, F., Klos, J., & Lique, F. 2011, *Physical Chemistry Chemical Physics (Incorporating Faraday Transactions)*, 13, 8204
 Faure, A., Valiron, P., Wernli, M., et al. 2005, *J. Chem. Phys.*, 122, 221102
 Faure, A., Crimier, N., Ceccarelli, C., et al. 2007, *A&A*, 472, 1029
 Faure, A., Wiesenfeld, L., Scribano, Y., & Ceccarelli, C. 2012, *MNRAS*, 420, 699
 Faure, A., & Josselin, E. 2008, *A&A*, 492, 257
 Goicoechea, J.R., Rodríguez-Fernández, N.J., Cernicharo, J. 2004, *ApJ*, 600, 214
 Goicoechea, J.R., Cernicharo, J., Karska, A. et al. 2012, *A&A*, submitted.
 González-Alfonso E., Cernicharo J., Bachiller R., Fuente A., 1995, *A&A*, 293, L9
 González-Alfonso, E., Cernicharo, J., Alcolea, J., Orlandi, M.A. 1998, *A&A*, 334, 1016
 Gonzalez-Alfonso, E., Smith, H.A., Fischer, J., Cernicharo, J. 2004, *ApJ*, 613, 247
 Grosjean, A., Dubernet, M.-L., & Ceccarelli, C. 2003, *A&A*, 408, 1197
 Green, S., Maluendes, S., & McLean, A. D. 1993, *ApJS*, 85, 181
 Guillón, G., & Stoecklin, T. 2012, *MNRAS*, 420, 579
 Guzmán, V., Pety, J., Goicoechea, J. R., Gerin, M., & Roueff, E. 2011, *A&A*, 534, A49
 Herczeg, G.J., Karska, A., Bruderer, S. et al. 2012, *A&A*, 540, 84
 Hogerheijde, M.R., Bergin, E.A., Brinch, C. et al. 2011, *Science*, 334, 338
 Kessler, M.F., et al. 1996, *A&A*, 315, L27
 Kristensen, L.E., van Dishoeck, E.F., Bergin, E.A. et al. 2012, *A&A*, in press.
 Klos, J., & Lique, F. 2008, *MNRAS*, 390, 239
 Klos, J., & Lique, F. 2011, *MNRAS*, 418, 271
 Lique, F., & Klos, J. 2008, *J. Chem. Phys.*, 128, 034306
 Lis, D.C., Phillips, T.G., Goldsmith, P.F. et al. 2010, *A&A*, 521, L26
 Melnick, G.J., et al. 2000, *ApJ*, 539, L77
 Menten, K.M., Melnick, G.J., Phillips, T.G., Neufeld, D.A. 1990, *ApJ*, 363, L27
 Menten, K.M., Melnick, G.J., Phillips, T.G. 1990b, *ApJ*, 350, L41
 Menten K., & Melnick G.J. 1991, *ApJ*, 377, 647
 Neufeld, D.A. & Kaufman, M.J. 1993 *ApJ*, 418, 263
 Neufeld, D.A.; Lepp, S., & Melnick, G.J. 1995, *ApJ*, 100, 132
 Neufeld, D.A., Gonzalez-Alfonso, E., Melnick, G.J. et al. 2011, *ApJ*, 727, L29
 Nordh, H.L., von Schéele, F., Frisk, U. et al. 2003, *A&A*, 402, L21
 Paganí, L., Vastel, C., Hugo, E., et al. 2009, *A&A*, 494, 623
 Parise, B., Belloche, A., Du, F., Güsten, R., & Menten, K. M. 2011, *A&A*, 526, A3
 Phillips, T.G., Kwan, J., and Huggins, P.J. 1980, in *IAU Symposium 87 : Interstellar Molecules*, ed. B.H. Andrew (Dordrecht: Reidel), p 21.
 Phillips, T. R., Maluendes, S., McLean, A. D., & Green, S. 1994, *J. Chem. Phys.*, 101, 5824
 Phillips, T. R., Maluendes, S., & Green, S. 1996, *ApJS*, 107, 467
 Pilbratt, G. L., Riedinger, J. R., Passvogel, T. et al. 2010, *A&A*, 518, L1
 Rothman, L. S., Gordon, I. E., Barbe, A., et al. 2009, *J. Quant. Spec. Radiat. Transf.*, 110, 533
 Royer, P., Decin, L., Wesson, R., Barlow, M.J. et al. 2010, *A&A*, 518, L145
 Troscompt, N., Faure, A., Wiesenfeld, L., Ceccarelli, C., & Valiron, P. 2009, *A&A*, 493, 687
 Troscompt, N., Faure, A., Maret, S., et al. 2009, *A&A*, 506, 1243
 Valiron, P., Wernli, M., Faure, A., et al. 2008, *J. Chem. Phys.*, 129, 134306
 van Dishoeck, E. F. 2004, *ARA&A*, 42, 119
 van Dishoeck, E. F., Kristensen, L. E., Benz, A. O., et al. 2011, *PASP*, 123, 138
 Waters, J. W. et al. 1980, *ApJ*, 235, 57
 Watson, D.M., Bohac, C.J., Hull, C. et al. 2007, *Nature*, 448, 1026
 Wernli, M., Valiron, P., Faure, A., et al. 2006, *A&A*, 446, 367
 Wernli, M., Wiesenfeld, L., Faure, A., & Valiron, P. 2007, *A&A*, 464, 1147
 Wernli, M., Wiesenfeld, L., Faure, A., & Valiron, P. 2007, *A&A*, 475, 391
 Yang, C.-H., Sarma, G., Parker, D. H., Ter Meulen, J. J., & Wiesenfeld, L. 2011, *J. Chem. Phys.*, 134, 204308

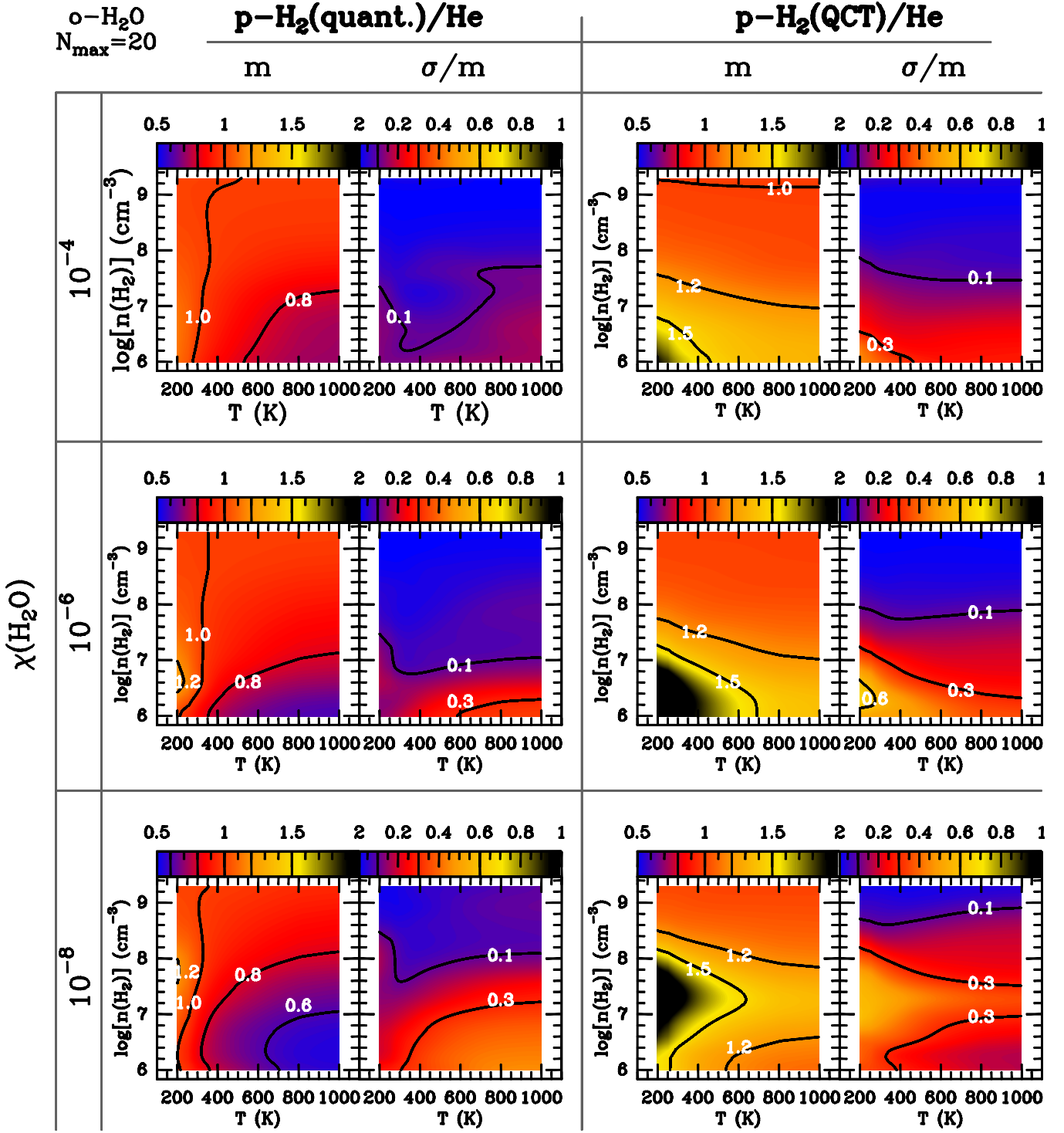
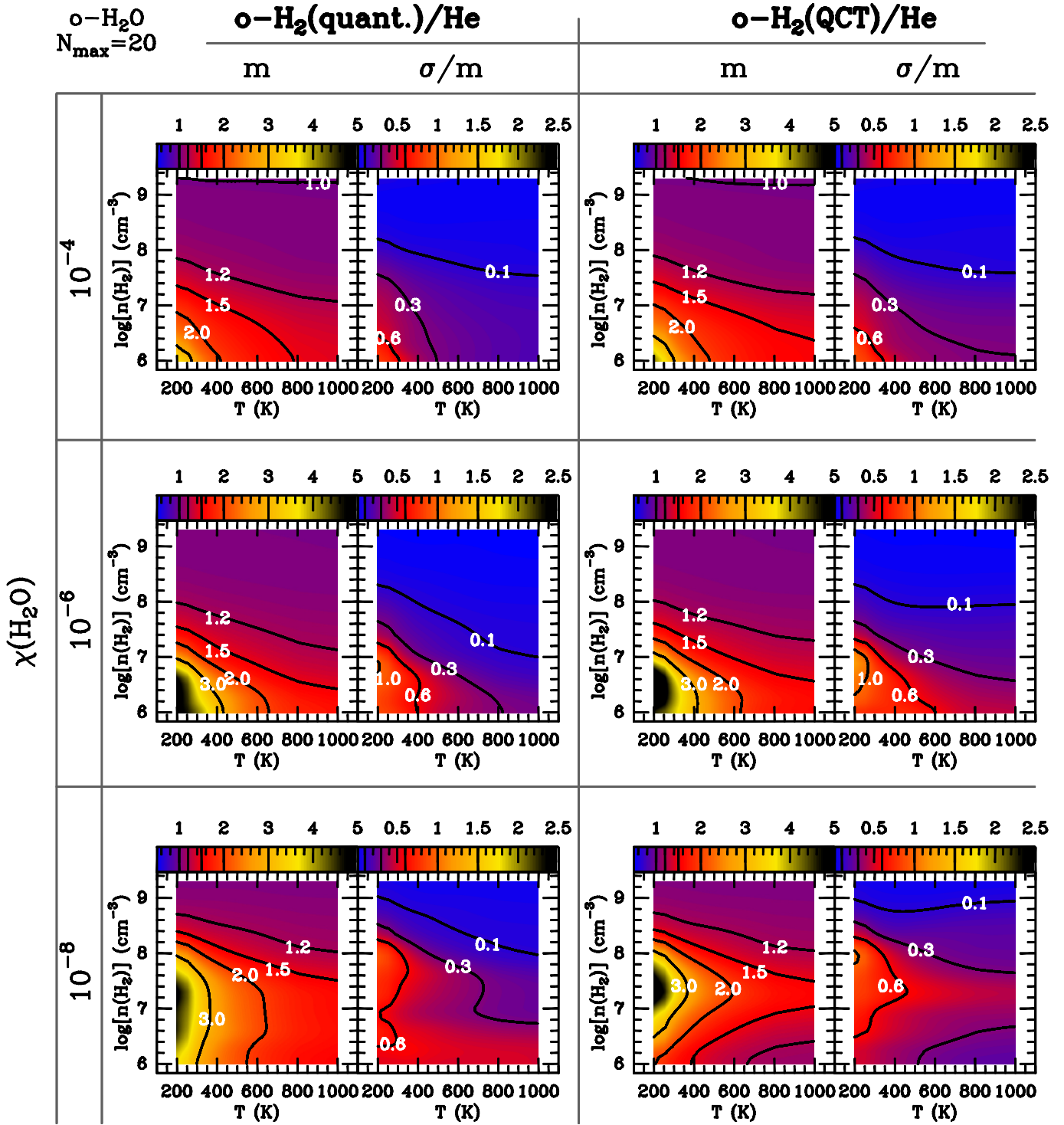


Fig. 2. Comparison of the mean (m) and normalised standard deviations (σ/m , given by eq. 4) for the ratios $\bar{I}^{quant.}/\bar{I}^{He}$ (left column) and $\bar{I}^{QCT}/\bar{I}^{He}$ (right column). The intensities \bar{I} are defined by eq. 1. The statistical analysis is performed on the lines that involve the first $N_{max} = 20$ o-H₂O energy levels. The comparison deals with p-H₂ CRC. The quantum CRC with p-H₂ are from Dubernet et al. (2009); Daniel et al. (2011), the quantum CRC with He from Green et al. (1993) and the QCT CRC are from Faure et al. (2007). In the case of the quantum CRC, the rates considered are the STS CRC with H₂ in $j_2 = 0$. The comparison is performed at the water abundances $\chi(\text{H}_2\text{O}) = 10^{-8}$, 10^{-6} and 10^{-4} (rows).

Fig. 3. Same as Fig. 2 but for the collisions that involve o-H₂.

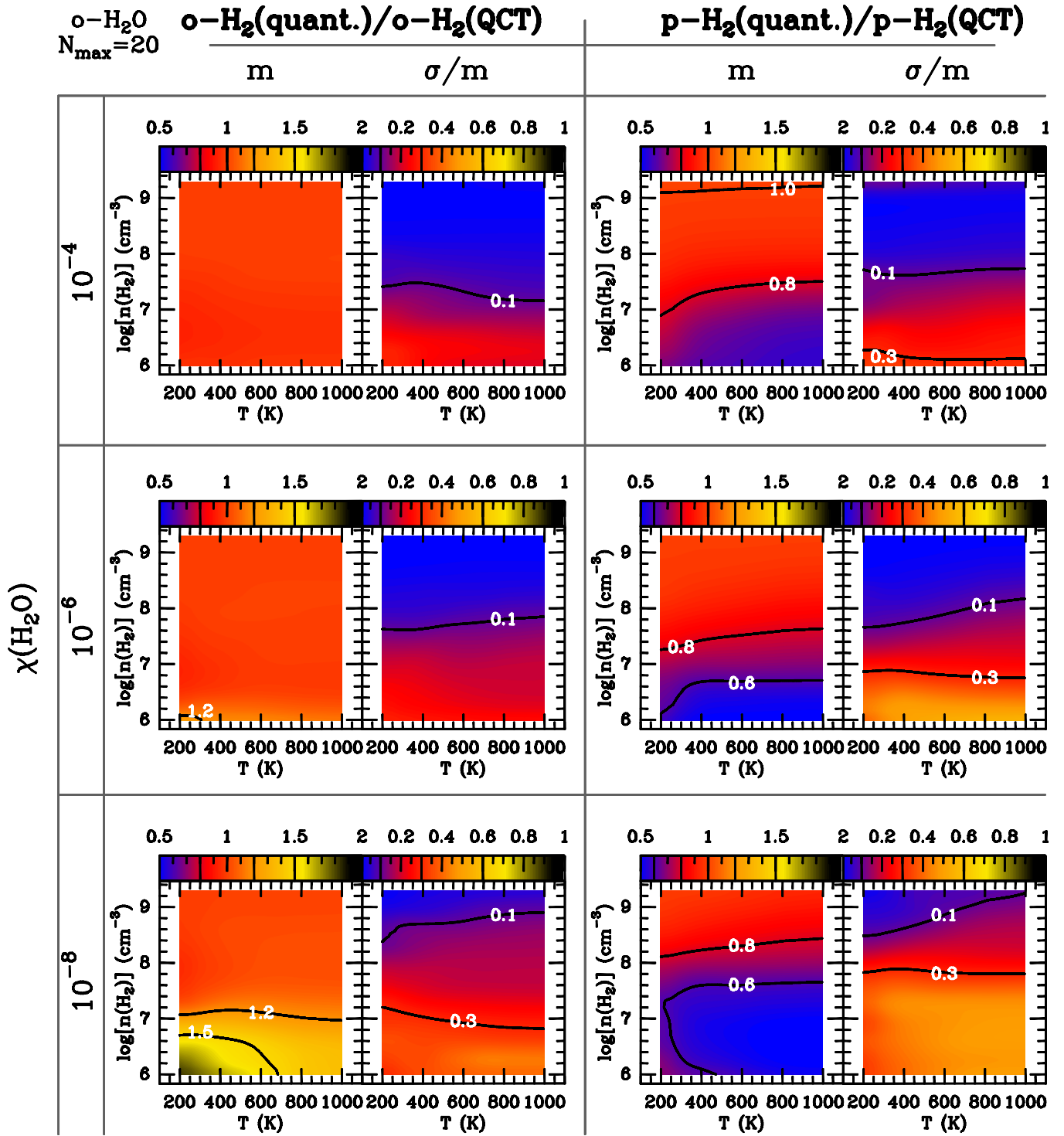


Fig. 4. Comparison of the results based on the quantum CRC from Dubernet et al. (2009); Daniel et al. (2011) with the QCT CRC from Faure et al. (2007), for both o-H₂ (left column) and p-H₂ (right column).

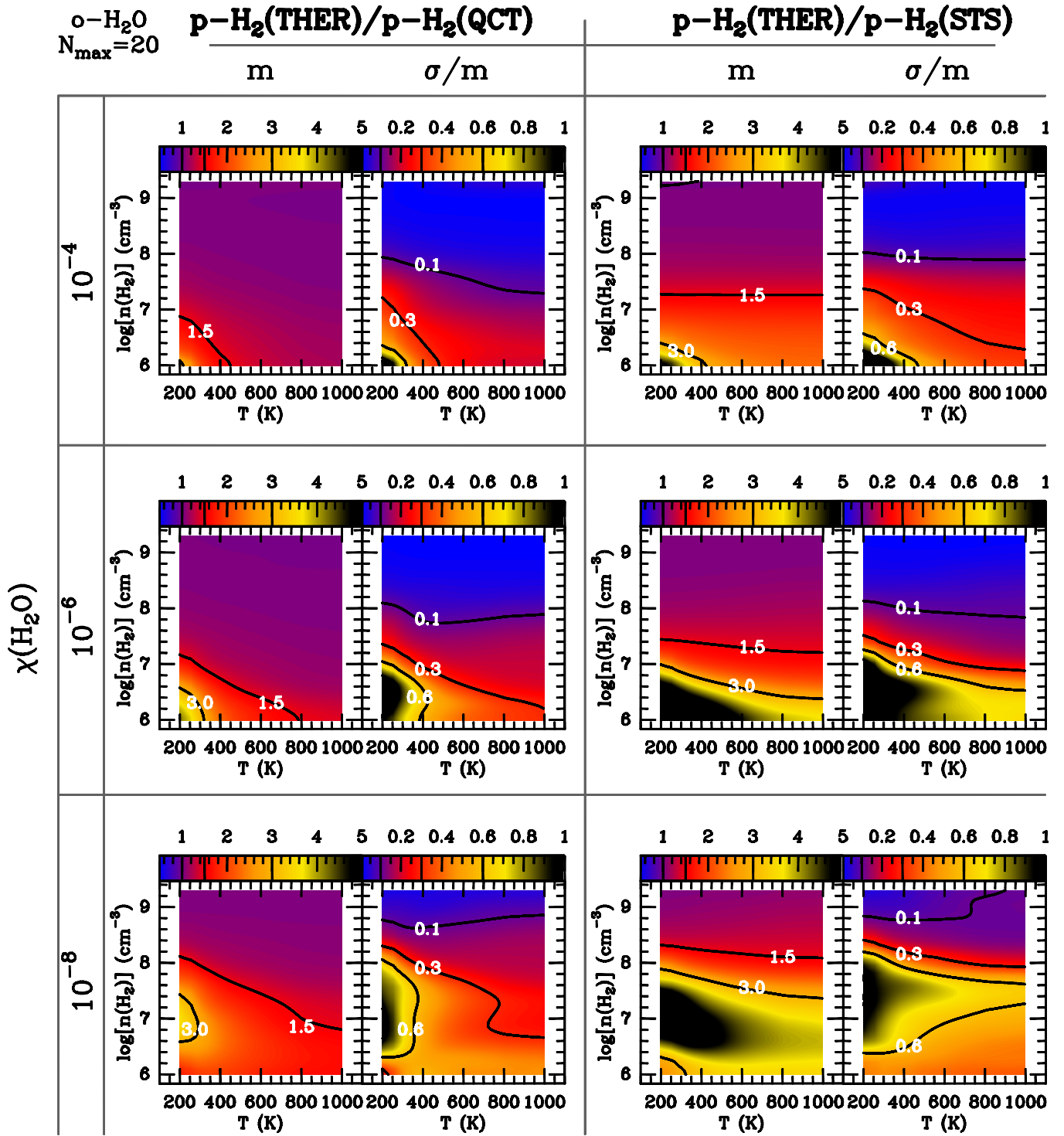


Fig. 7. Comparison of the results based on the QCT CRC from Faure et al. (2007) (left column) and state-to-state CRC from Dubernet et al. (2009); Daniel et al. (2011) (right column), both with the thermalized CRC from Dubernet et al. (2009); Daniel et al. (2011) for p-H₂.

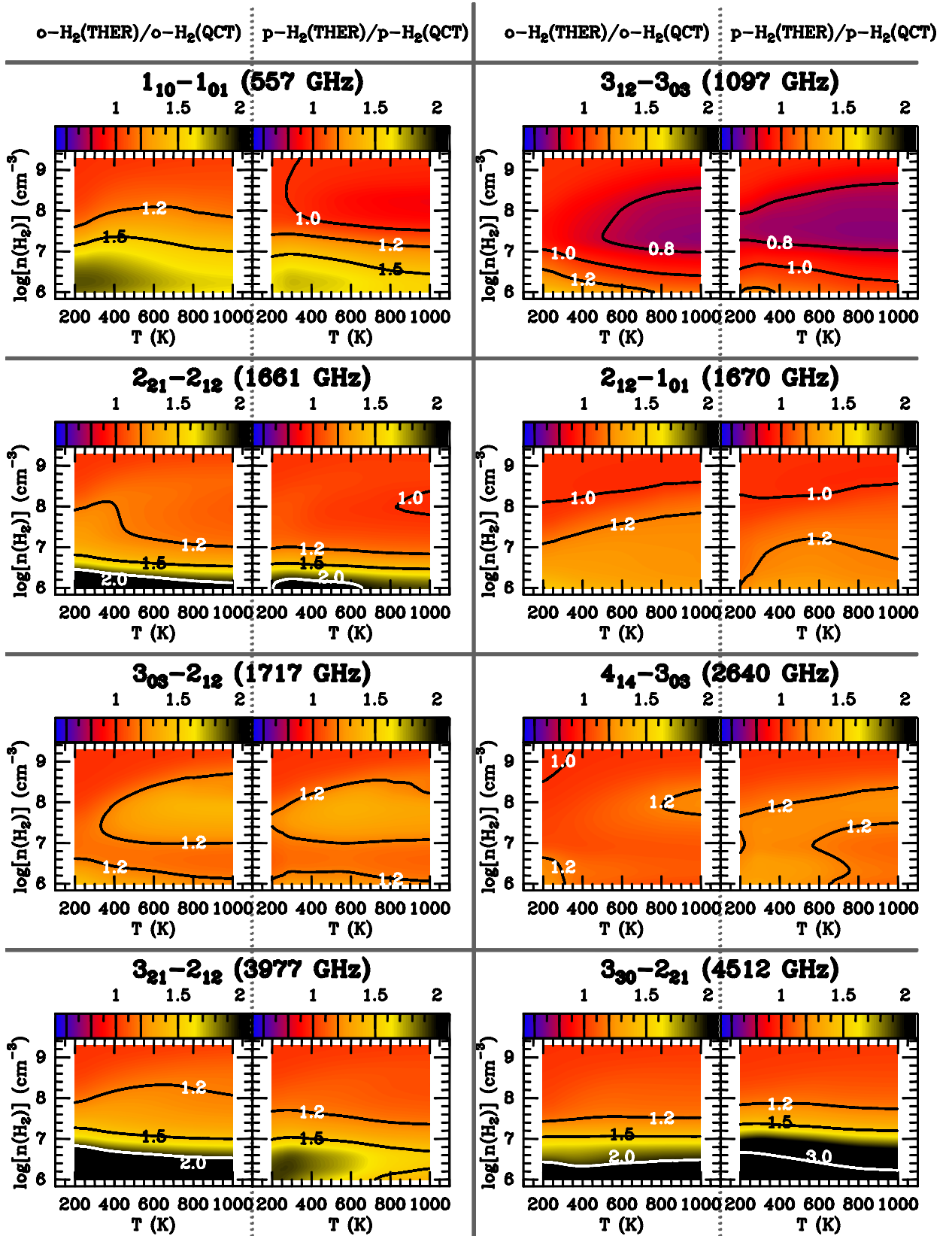


Fig. 9. Ratio $\bar{I}^{THER}/\bar{I}^{QCT}$ for a few transitions commonly observed with the Herschel satellite. The thermalized CRC are from Dubernet et al. (2009); Daniel et al. (2011) and the QCT CRC from Faure et al. (2007). The ratios are given for collisions that involve o-H₂ (left figure) and p-H₂ (right figure) in each panel.

transition	ν (GHz)	He	p-H ₂			o-H ₂		
			QCT	THER	STS	QCT	THER	STS
6 _{1,6} - 5 _{2,3}	22.	1.2(3)	1.1(3)	3.3(2)	4.2(2)	1.1(3)	2.9(2)	2.9(2)
4 _{1,4} - 3 _{2,1}	380.	5.2(6)	2.9(6)	2.8(6)	4.9(6)	1.5(6)	1.4(6)	1.4(6)
4 _{2,3} - 3 _{3,0}	448.	5.9(6)	3.9(6)	3.5(6)	6.1(6)	1.4(6)	1.5(6)	1.5(6)
1 _{1,0} - 1 _{0,1}	557.	8.1(7)	4.8(7)	3.4(7)	6.9(7)	3.1(7)	1.4(7)	1.4(7)
3 _{1,2} - 3 _{0,3}	1097.	6.7(8)	1.4(8)	2.7(8)	5.8(8)	1.1(8)	1.1(8)	1.1(8)
3 _{1,2} - 2 _{2,1}	1153.	2.2(8)	1.1(8)	1.1(8)	2.0(8)	4.9(7)	4.3(7)	4.3(7)
3 _{2,1} - 3 _{1,2}	1163.	9.1(8)	1.5(9)	3.5(8)	7.2(8)	7.4(8)	1.5(8)	1.5(8)
5 _{2,3} - 5 _{1,4}	1411.	1.6(9)	1.1(9)	6.6(8)	1.6(9)	4.3(8)	2.6(8)	2.6(8)
2 _{2,1} - 2 _{1,2}	1661.	1.9(9)	2.6(9)	9.7(8)	1.9(9)	1.4(9)	4.2(8)	4.2(8)
2 _{1,2} - 1 _{0,1}	1670.	1.3(9)	8.4(8)	6.6(8)	1.1(9)	6.7(8)	3.3(8)	3.3(8)
4 _{3,2} - 5 _{0,5}	1714.	2.2(8)	2.2(8)	1.4(8)	2.0(8)	2.2(8)	8.7(7)	8.7(7)
3 _{0,3} - 2 _{1,2}	1717.	1.8(9)	6.3(8)	8.6(8)	1.4(9)	4.6(8)	4.1(8)	4.1(8)
5 _{2,3} - 4 _{3,2}	1919.	1.8(9)	7.1(8)	8.0(8)	1.1(9)	3.0(8)	4.8(8)	4.8(8)
3 _{3,0} - 3 _{2,1}	2196.	4.6(9)	2.0(9)	2.5(9)	4.0(9)	1.0(9)	1.2(9)	1.2(9)
5 _{1,4} - 5 _{0,5}	2222.	6.4(9)	5.9(8)	3.1(9)	6.1(9)	4.2(8)	1.2(9)	1.2(9)
4 _{2,3} - 4 _{1,4}	2264.	7.1(9)	5.4(9)	3.3(9)	5.8(9)	1.9(9)	1.5(9)	1.5(9)
4 _{3,2} - 4 _{2,3}	2463.	1.0(10)	3.0(9)	4.7(9)	6.9(9)	2.2(9)	2.5(9)	2.5(9)
4 _{1,4} - 3 _{0,3}	2641.	9.9(9)	4.2(9)	4.9(9)	6.5(9)	3.0(9)	3.0(9)	3.0(9)
2 _{2,1} - 1 _{1,0}	2774.	1.1(10)	5.3(9)	5.0(9)	7.0(9)	4.2(9)	2.8(9)	2.8(9)
5 _{1,4} - 4 _{2,3}	2971.	1.6(10)	1.9(10)	7.4(9)	8.8(9)	7.5(9)	6.0(9)	6.0(9)
5 _{0,5} - 4 _{1,4}	3013.	1.7(10)	8.3(9)	8.7(9)	1.1(10)	5.5(9)	6.0(9)	6.0(9)
6 _{1,6} - 5 _{0,5}	3655.	3.9(10)	1.9(10)	2.0(10)	2.2(10)	1.2(10)	1.5(10)	1.5(10)
4 _{2,3} - 3 _{1,2}	3807.	4.6(10)	3.6(10)	2.4(10)	2.9(10)	2.1(10)	1.7(10)	1.7(10)
3 _{2,1} - 2 _{1,2}	3977.	4.3(10)	4.4(10)	2.1(10)	3.2(10)	3.9(10)	1.2(10)	1.2(10)
3 _{3,0} - 3 _{0,3}	4457.	1.3(10)	1.3(10)	9.7(9)	1.7(10)	6.7(9)	5.3(9)	5.3(9)
3 _{3,0} - 2 _{2,1}	4512.	1.0(11)	4.6(10)	4.4(10)	5.7(10)	3.1(10)	3.3(10)	3.3(10)
4 _{3,2} - 3 _{2,1}	5107.	2.0(11)	9.7(10)	8.6(10)	1.1(11)	5.5(10)	7.4(10)	7.4(10)
5 _{2,3} - 4 _{1,4}	6646.	4.9(11)	4.9(11)	1.3(11)	3.4(11)	8.8(10)	1.2(11)	1.2(11)
4 _{3,2} - 3 _{0,3}	7368.	5.1(11)	5.1(11)	8.2(10)	4.8(11)	8.5(10)	7.5(10)	7.6(10)

Table 1. Critical densities for the lines that involve the first 15th o-H₂O energy levels, at T = 200 K. The critical densities are given for the He CRC of Green et al. (1993), the QCT CRC of Faure et al. (2007) and the quantum CRC of Dubernet et al. (2009); Daniel et al. (2011). In the latter case, the values are given for both STS and thermalized CRC.

transition	ν (GHz)	λ (μ m)	E_u (K)	$\chi(\text{H}_2\text{O}) = 10^{-8}$		$X(\text{H}_2\text{O}) = 10^{-6}$		$X(\text{H}_2\text{O}) = 10^{-4}$	
				mean	σ/m	mean	σ/m	mean	σ/m
1 _{1,0} - 1 _{0,1}	557.	538.	61.	2.8	0.8	1.4	0.4	1.3	0.3
3 _{1,2} - 3 _{0,3}	1097.	273.	249.	3.2	0.7	2.7	0.8	2.3	1.1
3 _{2,1} - 3 _{1,2}	1163.	258.	305.	2.8	0.7	2.6	0.8	2.1	0.8
2 _{2,1} - 2 _{1,2}	1661.	180.	194.	2.5	0.6	2.1	0.6	1.5	0.3
2 _{1,2} - 1 _{0,1}	1670.	180.	114.	2.1	0.6	1.7	0.5	1.6	0.5
3 _{0,3} - 2 _{1,2}	1717.	175.	197.	2.2	0.5	2.0	0.7	1.2	0.4
3 _{3,0} - 3 _{2,1}	2196.	136.	411.	2.6	0.7	2.0	0.6	1.8	0.6
4 _{2,3} - 4 _{1,4}	2264.	132.	432.	2.9	0.6	2.3	0.8	2.0	0.8
4 _{1,4} - 3 _{0,3}	2640.	114.	323.	1.8	0.4	1.7	0.6	1.5	0.4
2 _{2,1} - 1 _{1,0}	2774.	108.	194.	2.5	0.7	2.5	0.9	2.0	0.5
5 _{1,4} - 4 _{2,3}	2971.	101.	575.	1.9	0.4	1.6	0.4	1.3	0.6
5 _{0,5} - 4 _{1,4}	3013.	99.	468.	1.7	0.3	1.6	0.5	1.6	0.6
6 _{1,6} - 5 _{0,5}	3655.	82.	644.	1.1	0.2	1.1	0.2	1.1	0.3
4 _{2,3} - 3 _{1,2}	3807.	79.	432.	2.4	0.4	2.0	0.7	1.8	0.6
3 _{2,1} - 2 _{1,2}	3977.	75.	305.	3.2	0.8	3.4	1.6	2.4	1.1
7 _{0,7} - 6 _{1,6}	4167.	72.	843.	0.5	0.2	0.7	0.2	0.8	0.1
3 _{3,0} - 3 _{0,3}	4457.	67.	411.	2.6	0.5	2.5	0.8	2.3	0.7
3 _{3,0} - 2 _{2,1}	4512.	66.	411.	2.4	0.4	2.1	0.7	1.9	0.6
6 _{2,5} - 5 _{1,4}	4600.	65.	796.	0.8	0.2	1.0	0.3	1.0	0.3
4 _{3,2} - 3 _{2,1}	5107.	59.	550.	1.2	0.4	1.3	0.3	1.0	0.3
4 _{4,1} - 3 _{3,0}	6076.	49.	702.	0.5	0.4	0.7	0.3	0.7	0.4
5 _{3,2} - 4 _{2,3}	6249.	48.	732.	0.5	0.6	0.8	0.3	0.8	0.3
5 _{2,3} - 4 _{1,4}	6646.	45.	642.	0.9	0.4	1.1	0.3	1.0	0.4
4 _{3,2} - 3 _{0,3}	7368.	41.	550.	1.7	0.2	1.5	0.4	1.3	0.2

Table 2. Mean values and normalised standard deviations for the ratios $\bar{I}^{\text{ortho}}/\bar{I}^{\text{para}}$ obtained with the thermalized CRC from Dubernet et al. (2009); Daniel et al. (2011). The parameters correspond to gas temperatures in the range $20 < T_k < 100$ K and $10^5 < n(\text{H}_2) < 2.10^8$ cm⁻³.

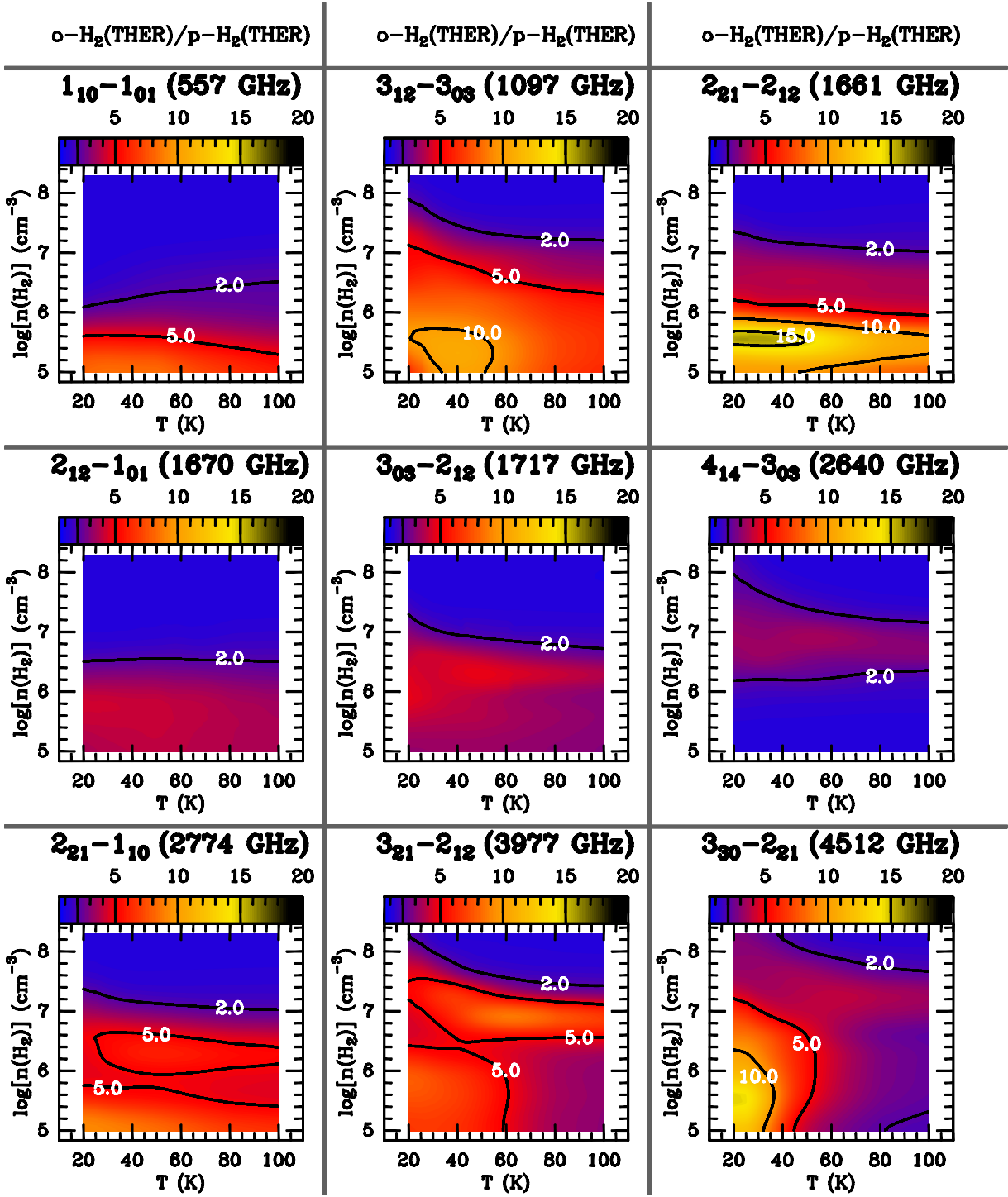


Fig. 14. Comparison of the ratio $\bar{I}^{ortho}/\bar{I}^{para}$ for a few o-H₂O transitions that involve its lowest energy levels. The results are derived from the thermalised CRC from Dubernet et al. (2009); Daniel et al. (2011) and are given for the temperature range $T_K = 20\text{--}100$ K.